Invisible low-frequency gravitons and the audio band

Massimo Giovannini*

Istituto Nazionale di Fisica Nucleare, Milan-Bicocca, 20126 Milan, Italy

(Received 28 June 2023; accepted 14 November 2023; published 4 December 2023)

The low-frequency gravitons correspond to typical wavelengths that left the Hubble radius during the early inflationary stages of expansion and reentered after matter radiation equality. Consequently the temperature and the polarization anisotropies of the cosmic microwave background constrain the tensor-to-scalar ratio in the aHz region but, since the audio band and the MHz domain are sensitive to the postinflationary expansion rate, the low-frequency determinations of the tensor-to-scalar ratio can be combined with the high-frequency constraints. In this framework we examine the possibility that the low-frequency gravitons remain invisible in the aHz region but are still potentially detectable at much higher frequencies. Because the number of e-folds associated with the exit of the cosmic microwave background wavelengths depends both on the slow-roll parameters and on the total expansion rate after inflation, this approach leads to a set of lower bounds on the tensor-to-scalar ratio.

DOI: 10.1103/PhysRevD.108.123508

I. INTRODUCTION

The tensor modes of the geometry affect all the angular power spectra of the cosmic microwave background (CMB) anisotropies but the distinctive feature of relic gravitons in the aHz region[1] should appear from the analysis of the polarization anisotropies that have been originally discovered in the first releases of the WMAP collaboration [1–3] and later confirmed by other ground based experiments as well as by the relatively recent observations of the Planck satellite [4]. However the low-frequency gravitons not only affect the E-mode but also the B-mode polarization which is instead absent in the case of curvature inhomogeneities; in spite of some claims subsequently withdrawn [5], so far there is no evidence for the presence of a B-mode polarization caused by the low-frequency gravitons. There are, of course, sources of B-mode polarization that have been successfully detected in the CMB like the one associated with the gravitational lensing of the primary anisotropies [6]. These B-mode signals are however not related with the ones generated by the relic gravitons in the aHz region. The current analyses suggest that the temperature and the polarization anisotropies of the CMB are caused by the curvature inhomogeneities that are Gaussian and (at least predominantly) adiabatic; these are, in a nutshell, the distinctive features of the so-called adiabatic paradigm whose formulation can be traced back to the pioneering analyses of Peebles and Yu [7]. In this framework various bounds on the aHz gravitons have been deduced both by the WMAP team [1–3] and by the subsequent experiments (see e.g. [8–10]).

In practice the bounds on the aHz gravitons take the form of limits on the so-called tensor-to-scalar ratio r_T since, in the adiabatic paradigm,[2] the production of relic gravitons is associated with decreasing frequency spectra whose amplitudes and slopes are simultaneously fixed at a conventional pivot wave number k_p by the relation $r_T = \mathcal{A}_T/\mathcal{A}_{\mathcal{R}}$, where $\mathcal{A}_T$ and $\mathcal{A}_{\mathcal{R}}$ denote, respectively, the amplitudes of the tensor and of the scalar power spectra. The lowest range of comoving frequencies corresponds therefore to $\nu = \mathcal{O}(\nu_p)$ where $\nu_p = k_p/(2\pi) = 3.092$ aHz and $k_p = 0.002$ Mpc^{-1}. All the CMB experiments setting limits on r_T are therefore constraining the aHz domain and these bounds will get progressively more stringent in the future. While the WMAP collaboration could set upper limits $r_T < \mathcal{O}(0.1)$, the most recent determinations suggest $r_T < \mathcal{O}(0.06)$ or even $r_T < \mathcal{O}(0.03)$ [8–10]. In the concordance scenario (often dubbed ΛCDM paradigm where Λ denotes the dark energy

*massimo.giovannini@cern.ch

[1]We shall be using the prefixes of the International System of Units so that, for instance, 1 aHz $= 10^{-18}$ Hz, 1 fHz $= 10^{-15}$ Hz and so on.

[2]Entropic (or nonadiabatic) modes are strictly absent in the minimal version of the concordance paradigm. Depending on the scenario the entropic modes can be up to five [11–14]. In the presence of nonadiabatic modes a tensor-to-scalar ratio must be introduced for each of the modes and for their correlations. We shall stick to the adiabatic paradigm also because its nonadiabatic extensions are strongly constrained [8–10].

component and CDM stands for the cold dark matter contribution) the spectral slope n_T and the slow-roll parameter ϵ are expressible in terms of r_T according to the so-called consistency relations stipulating that $n_T \simeq -2\epsilon \simeq -r_T/8$. The stochastic backgrounds of relic gravitons are however not peculiar of the ΛCDM case and have been actually suggested well before the formulation of any of the current scenarios aiming at a specific account of the early stages of the evolution of our Universe [15–17].

As already mentioned above, the frequencies $\mathcal{O}(\text{few})$ aHz correspond to wavelengths that left the Hubble radius well before the onset of the radiation-dominated phase and reentered after matter-radiation equality [18,19]. However, even assuming the presence of an early inflationary stage, the high-frequency range of the spectrum chiefly depends on the postinflationary evolution which is observationally unaccessible [20–22]. Nonetheless, the maximal comoving frequency of the relic graviton spectrum can be generally expressed as

$$\nu_{\max} = \overline{\nu}_{\max}(r_T, \mathcal{A}_{\mathcal{R}})/\mathcal{D}(\delta_i, \xi_i), \tag{1.1}$$

where $\overline{\nu}_{\max}$ depends on r_T and on the amplitude of curvature inhomogeneities $\mathcal{A}_{\mathcal{R}}$; in Eq. (1.1) $\mathcal{D}(\delta_i, \xi_i)$ accounts for the postinflationary evolution and its specific form is not essential for the purposes of this introduction (see, however, the discussion of Appendix A). Since there could be various distinct epochs, the subscripts appearing in the expansion rates (i.e. δ_i) and in their relative durations (i.e. ξ_i) count the successive expanding phases. Assuming that all the δ_i go to 1 we have that, within the present notations, $\nu_{\max} \to \overline{\nu}_{\max} = \mathcal{O}(270)(r_T/0.06)^{1/4}$ MHz and Eq. (1.1) eventually reproduces the maximal frequency of the spectrum obtained when the inflationary stage of expansion is suddenly replaced by a radiation-dominated phase. In this case the spectral energy density in critical units [denoted hereunder[3] by $h_0^2\Omega_{gw}(\nu, \tau_0)$] is quasiflat as a function of the comoving frequency. If the postinflationary expansion rate is different from radiation, then $h_0^2\Omega_{gw}(\nu, \tau_0)$ is generally not flat and whenever the expansion rate is faster than radiation the spectral energy density in critical units decreases. Conversely when the expansion rate is slower than radiation $h_0^2\Omega_{gw}(\nu, \tau_0)$ increases as a function ν. As we shall see the postinflationary evolution also affect the maximal frequency of the spectrum illustrated in Eq. (1.1): $\nu_{\max}$ is either larger or smaller than $\mathcal{O}(270)$ MHz depending on the expansion rate (see, in this respect, Appendix A and the discussion therein).

Also the total number of inflationary e-folds depends on the postinflationary evolution and if we focus on the number of e-folds associated with the crossing of the CMB scales $k = \mathcal{O}(k_p)$ we have that[4]

$$N_k = \mathcal{O}(60) + \frac{1}{4}\ln\left(\frac{r_T}{0.06}\right) + \ln \mathcal{D}(\delta_i, \xi_i), \tag{1.2}$$

where the consistency relations have been assumed. Since N_k enters directly the predictions of the spectral index and of the tensor-to-scalar ratio we can conclude that the postinflationary evolution ultimately affects all the inflationary observables including the spectral index of curvature inhomogeneities.

In short the main purpose of this analysis is to answer the following question: by how much can we reduce r_T without suppressing the signal in the audio and in the MHz band? From a phenomenological viewpoint the interplay between the aHz region and the high-frequency range rests on various observations that are progressively limiting the degree of arbitrariness of the high-frequency shape of $h_0^2\Omega_{gw}(\nu, \tau_0)$. Starting in 2004 the wideband detectors obtained a series of limits on the spectral energy density of the relic gravitons [23–26] for a typical pivot frequency smaller than 300 Hz. While different spectral slopes lead to slightly modified bounds we should have that $h_0^2\Omega_{gw}(\nu, \tau_0) < \mathcal{O}(10^{-9})$ for comoving frequencies falling in the audio band (i.e. between few Hz and 10 kHz). Moreover the pulsar timing arrays (PTAs) recently reported an evidence potentially attributed to the relic gravitons: the four collaborations currently investigating the nHz band (between few nHz and 0.1 μHz) report compatible determinations of $h_0^2\Omega_{gw}(\nu, \tau_0)$ [27–30] implying $10^{-9.09} \leq h_0^2\Omega_{gw}(\nu, \tau_0) \leq 10^{-8.07}$. There are finally indirect bounds on the high-frequency branch of the spectrum coming from big bang nucleosynthesis: since the additional relativistic species increase the expansion rate at the nucleosynthesis time it is possible to set a bound on the possible presence of relic gravitons and this constraint is customarily phrased in terms of a specific integral of $h_0^2\Omega_{gw}(\nu, \tau_0)$ [31–33] between 10^{-2} nHz and $\nu_{\max}$ whose precise value depends, as already stressed in Eq. (1.1), on the details of the postinflationary evolution.

Equations (1.1) and (1.2) suggest that the low-frequency limits on r_T are closely related with the high-frequency determinations through $\mathcal{D}(\delta_i, \xi_i)$. Some time ago [34] it has been pointed out that the low-frequency and high-frequency determinations of the relic graviton backgrounds could be eventually combined in a synergic perspective in order to improve the determinations of the cosmological

[3]The spectral energy density in critical units (specifically defined later on) is denoted by $\Omega_{gw}(\nu, \tau_0)$. It is however customary to deal directly with $h_0^2\Omega_{gw}(\nu, \tau_0)$ since the latter quantity does not depend on the indetermination of the present Hubble rate. We also note that the present value of the scale factor is normalized as $a_0 = 1$ and this means that at τ_0 the comoving and the physical frequencies coincide.

[4]In the present paper $\ln x$ denotes the natural logarithm of a generic variable x; $\log x$ denotes instead the common logarithm of the same quantity. As a consequence of Eq. (1.2), as we shall see, it follows that $N_k > \mathcal{O}(60)$ when the postinflationary evolution is slower than radiation while $N_k < \mathcal{O}(60)$ is the postinflationary evolution is faster than radiation.

parameters. In the concordance paradigm the low-frequency signal is often maximized by assuming the largest r_T compatible with the current data. In this analysis we instead focus on the possibility that $r_T(k_p) \ll 0.06$ and this choice implies that the low-frequency gravitons might be eventually invisible in the aHz region without jeopardizing the possibility of a larger signal in the audio band or even in the GHz domain.

The layout of this paper is the following. In Sec. II we introduced the timeline of the comoving horizon and the connections between $r_T(k,\tau)$ and $\Omega_{gw}(k,\tau)$ in the different frequency domains relevant for the present analysis. In view of its relevance, the case of single-field scenarios satisfying the consistency relations is also discussed at the end of Sec. II. In Sec. III the most constraining physical situations are addressed in preparation for the bounds of Sec. IV where a number of more specific examples is also presented. Section V contains the concluding remarks and, to avoid digressions, some useful results have been collected in Appendices A and B.

II. THE TIMELINE OF THE COMOVING HORIZON AND r_T

A. The timeline of the comoving horizon

The expressions of the maximal frequency and of the number of e-folds given in Eqs. (1.1) and (1.2) follow from the general form of the comoving horizon when the inflationary stage is supplemented by a postinflationary evolution that does not necessarily coincide with the radiation-dominated plasma. In Fig. 1 we illustrate the comoving horizon as a function of the scale factor (common logarithms are assumed on both axes). The thick (diagonal) line at the left of the cartoon corresponds to the inflationary evolution and the *filled squares* define the exit of a given (comoving) wavelength while *the disks* in the right portion of the plot denote reentry of the selected scale. According to Fig. 1 the wavelengths smaller than λ_r reenter before radiation dominance while the wavelengths $\lambda > \lambda_r$ (illustrated by a shaded stripe) reenter between the onset of radiation dominance and the epoch of matter-radiation equality.

For $\lambda < \lambda_r$ the wavelength $\mathcal{O}(\lambda_{\rm min})$ corresponds to comoving frequencies $\mathcal{O}(\nu_{\rm max})$, i.e. the maximal frequency of the spectrum already mentioned in Eq. (1.1). The scales $\lambda_r < \lambda < \lambda_{eq}$ were still larger than the comoving horizon prior to matter-radiation equality and exited about N_k e-folds before the end of inflation; the corresponding wave numbers range therefore between 0.05 and 0.002 Mpc^{-1} and the corresponding number of e-folds is given in Eq. (1.2). By considering the timeline of Fig. 1 we can obtain the specific form of N_k which is in fact derived in Appendix A [see, in particular, Eq. (A10)]:

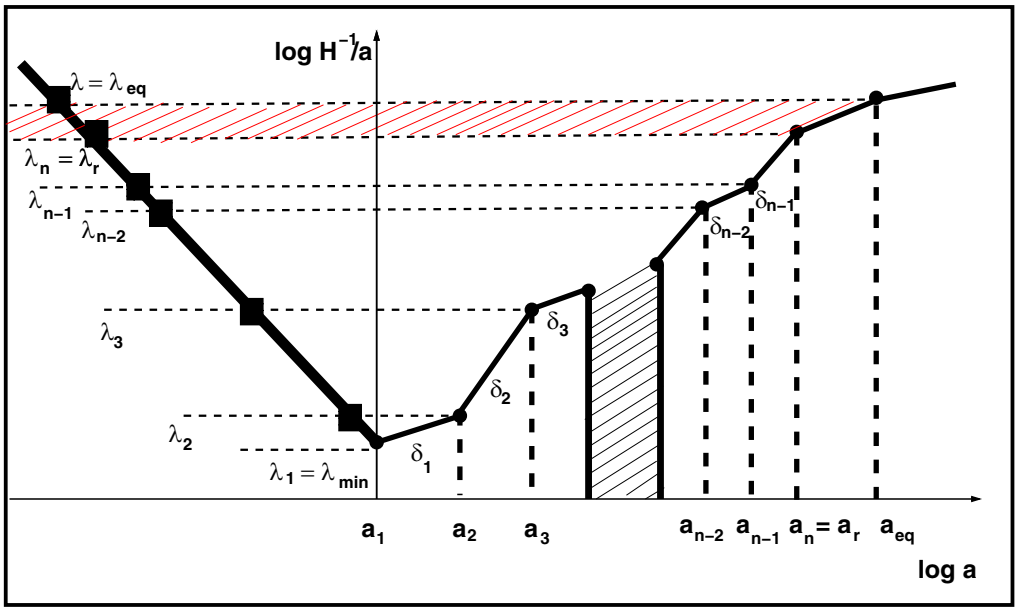

FIG. 1. The common logarithm of the comoving horizon is illustrated as a function of the common logarithm of the scale factor. The left region of the cartoon corresponds to the inflationary evolution while the postinflationary stage occurs for $a > a_1$. Between a_1 and a_n there are $n-1$ successive sages of expansion characterized by the rates δ_i; we consistently use the convention that a_n coincides with a_r (i.e. the beginning of the conventional radiation-dominated evolution). It is also understood throughout the discussion that the postinflationary stage is bounded by the curvature scale of big bang nucleosynthesis so that $H_r \geq 10^{-44} M_P$. The presence of a nonstandard evolution between a_1 and a_n potentially modifies the number of e-folds as well as the spectral energy density of the produced gravitons. The shaded stripe corresponds to the bunch of wavelengths exiting the horizon during inflation and reentering between radiation dominance and matter-radiation equality.

$$N_k = 59.4 + \frac{1}{4}\ln\left(\frac{\epsilon_k}{0.001}\right) - \ln\left(\frac{k}{0.002\ \mathrm{Mpc}^{-1}}\right) + \frac{1}{2}\sum_{i}^{n-1}\left(\frac{\delta_i - 1}{\delta_i + 1}\right)\ln\xi_i - \frac{1}{2}\ln\left(\frac{H_1}{H_k}\right). \tag{2.1}$$

Some of the numerical factors discussed in Appendix A have been purposely neglected in Eq. (2.1) and ϵ_k is the value of the slow-roll parameter when the scale $\mathcal{O}(k^{-1})$ crosses the comoving horizon. In Eq. (2.1) the various ξ_i measure the duration of each postinflationary stage of expansion and since the expansion rate is always decreasing we conclude that[5]

$$\xi_i = \frac{H_{i+1}}{H_i} < 1, \qquad \prod_{i=1}^{n-1}\xi_i = \xi_1\xi_2\ldots\xi_{n-2}\xi_{n-1} = \xi_r = H_r/H_1 < 1. \tag{2.2}$$

The fourth term at the right-hand side of Eq. (2.1) is the natural logarithm of $\mathcal{D}^{-1}(\delta_i, \xi_i)$ already introduced in Eq. (A4) and here rewritten for immediate convenience:

$$\mathcal{D}(\delta_i, \xi_i) = \prod_{i=1}^{n-1}\xi_i^{-\frac{(\delta_i-1)}{2(\delta_i+1)}}. \tag{2.3}$$

Concerning Eqs. (2.1)–(2.3) we remark that a reduction of ϵ_k also implies a reduction of N_k, but this effect is overall secondary in view of the scales of the problem: for a reduction of 4 orders of magnitude of ϵ_k we have that N_k gets reduced of 1 order of magnitude, which is practically immaterial for the present purposes. In case the consistency relations are enforced, a reduction of ϵ_k also implies a suppression of r_T.

If the postinflationary plasma is only dominated by radiation then in Eq. (2.3) all the δ_i go to 1 and the fourth term in Eq. (2.1) disappears. Conversely when some of the δ_i are smaller than 1 then the expansion rate gets slower than radiation and N_k increases. For $\delta_i > 1$ we may have also the opposite effect suggesting an overall reduction of N_k. However, as discussed in Sec. III, when $\delta_i > 1$ the spectral energy density is generally decreasing and a large spectral energy density at high and intermediate frequencies is not expected. In both situations, as stressed in Appendix B, the Hubble rate at the exit of the given scale [H_k in Eq. (2.1)] coincides in practice with H_1 (i.e. the expansion rate at the end of inflation) so that the last term in Eq. (2.1) does not contribute to N_k.

[5]Note that $\xi_{n-1} = H_n/H_{n-1}$; but $H_n = H_r$ since, by construction, the value of a_n coincides with a_r, i.e. the scale factor at radiation dominance.

The timeline of Fig. 1 also determines the expression of the maximal frequency ν_{max} [see Eq. (1.1)] where $\overline{\nu}_{\mathrm{max}}$ now corresponds to the maximal frequency in the case where all the $\delta_i \to 1$. The value of $\overline{\nu}_{\mathrm{max}}$ can then be estimated in the case of a postinflationary evolution dominated by radiation and it is given by

$$\overline{\nu}_{\mathrm{max}} = 195.38\mathcal{C}(g_s, g_\rho)\left(\frac{\mathcal{A}_\mathcal{R}}{2.41\times10^{-9}}\right)^{1/4} \times \left(\frac{\epsilon_k}{0.001}\right)^{1/4}\left(\frac{h_0^2\Omega_{R0}}{4.15\times10^{-5}}\right)^{1/4}\ \mathrm{MHz}. \tag{2.4}$$

Equation (2.4) does not assume a specific relation between ϵ_k and r_T; however, if the consistency relations are enforced, then we can always trade ϵ_k for r_T and the value of $\overline{\nu}_{\mathrm{max}}$ becomes[6]

$$\overline{\nu}_{\mathrm{max}} = 271.93\mathcal{C}(g_s, g_\rho)\left(\frac{\mathcal{A}_\mathcal{R}}{2.41\times10^{-9}}\right)^{1/4}\left(\frac{r_T}{0.06}\right)^{1/4} \times \left(\frac{h_0^2\Omega_{R0}}{4.15\times10^{-5}}\right)^{1/4}\ \mathrm{MHz}. \tag{2.5}$$

B. The spectral energy density and the tensor-to-scalar ratio

For typical wavelengths larger than the Hubble radius (see Fig. 1) the tensor to scalar ratio is practically constant while the spectral energy density is suppressed. In the opposite limit the two quantities are both time dependent. Moreover, while the actual definition of r_T is largely unambiguous (except for the conventional choice of the pivot scale) the different prescriptions of the energy density do not generally agree for typical wavelengths larger than the Hubble radius. However, as recently pointed out [35], a consistent definition of the energy momentum pseudotensor follows from the variation of the second-order action with respect to the background metric. This approach, originally suggested in [36], must be combined with an appropriate averaging scheme [35] (see also [37,38]). In the case of the relic gravitons the averaging of the different combinations of the field operators follows from the quantum mechanical expectation values [34,35,39] so that the spectral energy density in critical units is eventually given by

$$\Omega_{gw}(k,\tau) = \frac{1}{24H^2a^2}[Q_T(k,\tau) + k^2P_T(k,\tau)], \tag{2.6}$$

[6]As also discussed in Appendix A, the impact of $\mathcal{C}(g_s, g_\rho)$ is minor; for typical values of the late-time parameters (i.e. $g_{\rho,r} = g_{s,r} = 106.75$ and $g_{\rho,eq} = g_{s,eq} = 3.94$) we have that $\mathcal{C}(g_s, g_\rho) = 0.7596$ and the determination of $\overline{\nu}_{\mathrm{max}}$ of Eq. (2.5) moves from $\overline{\nu}_{\mathrm{max}} = 271.93$ to 206.53 MHz.

and it depends both on the wave number and on the conformal time coordinate τ; $a(\tau)$ denotes the scale factor of a conformally flat background geometry and H is the standard Hubble rate which is also related to its conformal time counterpart as $\mathcal{H} = aH$. We recall, in this respect, that $\mathcal{H} = a'/a$ where the prime denotes a derivation with respect to τ. The two tensor power spectra appearing in Eq. (2.6) are

$$P_T(k,\tau) = \frac{4\ell_P^2}{\pi^2}k^3|F_k(\tau)|^2, \qquad Q_T(k,\tau) = \frac{4\ell_P^2}{\pi^2}k^3|G_k(\tau)|^2. \tag{2.7}$$

In Eq. (2.7) the mode functions $F_k(\tau)$ and $G_k(\tau)$ obey

$$G_k = F_k', \qquad G_k' = -2\mathcal{H}G_k - k^2F_k, \tag{2.8}$$

The amplitude of the tensor power spectra is related to the one of the curvature inhomogeneities via the tensor-to-scalar ratio which is, in general, scale dependent and time dependent:

$$r_T(k,\tau) = P_T(k,\tau)/P_{\mathcal{R}}(k,\tau), \qquad P_{\mathcal{R}}(k,\tau) = \frac{k^3}{2\pi^2}|\overline{F}_k(\tau)|^2. \tag{2.9}$$

From Eqs. (2.7) and (2.9) we therefore have that $r_T(k,\tau)$ can also be written as

$$r_T(k,\tau) = 8\ell_P^2|F_k(\tau)|^2/|\overline{F}_k(\tau)|^2. \tag{2.10}$$

In Eqs. (2.9) and (2.10) the mode functions $\overline{F}_k$ and $\overline{G}_k$ are associated with the curvature inhomogeneities and their evolution is formally similar to the one of Eq. (2.8)

$$\overline{G}_k = \overline{F}_k', \qquad \overline{G}_k' = -2\mathcal{F}\overline{G}_k - k^2\overline{F}_k, \tag{2.11}$$

where now $\mathcal{F} = z'/z$. The explicit form of $z(\tau)$ depends on the matter content when the corresponding wavelengths crossed the comoving horizon. In the case of single-field models $z = z_\varphi = a\varphi'/\mathcal{H}$ while for an irrotational relativistic fluid the term $k^2\overline{F}_k$ in Eq. (2.11) gets modified as $c_{st}^2k^2\overline{F}_k$; furthermore $z = z_t = a^2\sqrt{\rho_t + p_t}/(\mathcal{H}c_{st})$ [40] where p_t and ρ_t are, respectively, the total pressure and the total energy density of the relativistic fluid.

1. Wavelengths larger than the Hubble radius

Since the initial conditions of the Einstein-Boltzmann hierarchy (required for the calculations of the temperature and polarization anisotropies) are customarily set well before matter-radiation equality, Eqs. (2.9) and (2.10) must be computed when the relevant wavelengths are larger than the Hubble radius[7] i.e. for $\tau_{ex} \leq \tau < \tau_{re}$ and $k \ll aH$. In this regime Eqs. (2.8) and (2.11) are independently solved and the result is

$$F_k(\tau) = \frac{e^{-ik\tau_{ex}}}{a_{ex}\sqrt{2k}}\mathcal{Q}_k(\tau_{ex},\tau), \qquad \overline{F}_k(\tau) = \frac{e^{-ik\tau_{ex}}}{z_{ex}\sqrt{2k}}\overline{\mathcal{Q}}_k(\tau_{ex},\tau), \tag{2.12}$$

where the subscripts imply that the various quantities are evaluated when $\tau \to \tau_{ex}$ (i.e. when the relevant wavelengths cross the comoving horizon fro $a < a_1$ in Fig. 1). The functions $\mathcal{Q}_k(\tau_{ex},\tau)$ and $\overline{\mathcal{Q}}_k(\tau_{ex},\tau)$ are defined as

$$\mathcal{Q}_k(\tau_{ex},\tau) = 1 - (ik + \mathcal{H}_{ex})a_{ex}^2\int_{\tau_{ex}}^{\tau}\frac{\tau'}{a^2(\tau')},$$
$$\overline{\mathcal{Q}}_k(\tau_{ex},\tau) = 1 - (ik + \mathcal{F}_{ex})z_{ex}^2\int_{\tau_{ex}}^{\tau}\frac{\tau'}{z^2(\tau')}. \tag{2.13}$$

The results of Eqs. (2.12) and (2.13) follow by imposing the appropriate (quantum mechanical) initial conditions for $\tau < \tau_{ex}$ and by then solving Eqs. (2.8) and (2.11) across τ_{ex}. If we then insert Eqs. (2.12) and (2.13) into Eq. (2.10), then we obtain the explicit form of $r_T(k,\tau)$ valid for $k < aH$ and $\tau_{ex} \leq \tau < \tau_{re}$

$$r_T(k,\tau) = 8\ell_P^2\left(\frac{z_{ex}}{a_{ex}}\right)^2\frac{|\mathcal{Q}_k(\tau_{ex},\tau)|^2}{|\overline{\mathcal{Q}}_k(\tau_{ex},\tau)|^2}. \tag{2.14}$$

In the case of single field inflationary models and for the timeline of the comoving horizon illustrated in Fig. 1 we obtain[8]

$$r_T(k,\tau) = 8\ell_P^2\left(\frac{\dot{\varphi}^2}{H^2}\right)_{ex} \simeq 16\epsilon_k, \qquad \epsilon_k = -\left(\frac{\dot{H}}{H^2}\right)_{ex}, \tag{2.15}$$

since $\mathcal{Q}_k(\tau_{ex},\tau) \simeq \overline{\mathcal{Q}}_k(\tau_{ex},\tau) \to 1$ for the timeline of Fig. 1. The result of Eq. (2.15) follows if the initial conditions of the scalar and tensor mode functions are set when the background is already inflating; this means, in practice, that the total number of e-folds is larger than N_k [see also

[7] Indeed, before matter-radiation equality, $r_T(k,\tau)$ is used to set the initial conditions of the Einstein-Boltzmann hierarchy in CMB applications when the relevant wavelengths are still larger than the comoving horizon.

[8] In Eq. (2.15) the crossing condition $\tau_{ex} \simeq 1/k$ has been used. We also recall that, in the case of single-field case, from the Friedmann equations $2\dot{H} = -\ell_P^2\dot{\varphi}^2$; to get Eq. (2.15) we must also use the identity $(\varphi'/\mathcal{H}) = (\dot{\varphi}/H)$.

Eq. (2.1)]. In case the total number of e-folds is close to N_k the field operators corresponding to the scalar and tensor modes are not necessarily in the vacuum [41,42] and the protoinflationary transition can break the consistency relations. The tensor-to-scalar ratio of Eq. (2.15) will then include a dependence upon the sound speed of the preinflationary phonons; instead of $r_T(k,\tau) \simeq 16\epsilon_k$ we will have $r_T(k,\tau) \simeq 16\epsilon_k c_{st}$.

According to Eq. (2.15) the tensor-to-scalar ratio is approximately constant for wavelengths larger than the Hubble radius; in the same limit the spectral energy density of Eq. (2.6) is instead suppressed and from Eq. (2.12) we can show that

$$\Omega_{gw}(k,\tau) = \frac{k^4}{12\pi^2 H^2 \overline{M}_P^2 a^2 a_{ex}^2}\left[|\mathcal{Q}_k(\tau_{ex},\tau)|^2 + \frac{|\mathcal{Q}_k'(\tau_{ex},\tau)|^2}{k^2}\right], \tag{2.16}$$

where $\overline{M}_P = M_P/\sqrt{8\pi}$. Since the integral appearing in $Q_k(\tau_{ex},\tau)$ can be evaluated by parts

$$\int_{\tau_{ex}}^{\tau} \frac{d\tau'}{a^2(\tau')} = \frac{1}{3-\overline{\epsilon}}\left(\frac{1}{a^3 H} - \frac{1}{a_{ex}^3 H_{ex}}\right),$$
$$\overline{\epsilon} = \int_{\tau_{ex}}^{\tau} d\tau' \frac{\epsilon(\tau')}{a^2(\tau')} \Big/ \int_{\tau_{ex}}^{\tau} \frac{d\tau'}{a^2(\tau')}, \tag{2.17}$$

inserting Eq. (2.17) into Eq. (2.16) (and bearing in mind that $H_{ex} a_{ex} \simeq k$) the spectral energy density in critical units becomes

$$\Omega_{gw}(k,\tau) = \frac{2|k\tau|^2}{3\pi}\left(\frac{H_{ex}}{M_P}\right)^2 \mathcal{M}_k(\tau,\overline{\epsilon}),$$
$$\mathcal{M}_k(\tau,\overline{\epsilon}) = 1 + 2\left(\frac{a_{ex}}{a}\right)^2 + \frac{2}{(3-\overline{\epsilon})^2}\left[\left(\frac{a_{ex}}{a}\right)^2 k\tau - 1\right]^2$$
$$- \frac{2}{(3-\overline{\epsilon})}\left[\left(\frac{a_{ex}}{a}\right)^2 k\tau - 1\right], \tag{2.18}$$

implying, as expected, that $\Omega_{gw}(k,\tau)$ is suppressed in the two concurrent limits $\tau_{ex} \leq \tau < \tau_{re}$ and $k\tau \ll 1$. We finally stress that Eq. (2.17) holds for $\overline{\epsilon} \neq 3$ since for $\overline{\epsilon} \to 3$ there is a logarithmic enhancement that is irrelevant in this case but that must be taken into account when the wavelengths are shorter than the Hubble radius. Only if $a^2(\tau) \simeq 1/\mathcal{H}$ the contribution of the integrand of Eq. (2.17) is relevant; it corresponds to an extended stiff phase and, in this case, the spectral energy density and the other observables inherit a logarithmic correction.

2. Wavelengths shorter than the Hubble radius

When the wavelengths are shorter than the Hubble radius $F_k(\tau)$ and $G_k(\tau)$ exhibits standing oscillations for $\tau \geq \tau_{re}$

$$F_k(\tau) = \frac{e^{-ik\tau_{ex}}}{a\sqrt{2k}}\mathcal{Q}_k(\tau_{ex},\tau_{re})\left(\frac{a_{re}}{a_{ex}}\right)$$
$$\times\left\{\frac{\mathcal{H}_{re}}{k}\sin(k\Delta\tau) + \cos(k\Delta\tau)\right\}, \qquad \Delta\tau = (\tau - \tau_{re}), \tag{2.19}$$

where $\mathcal{Q}_k(\tau_{ex},\tau_{re})$ has been already defined in Eq. (2.13) and it is now evaluated for $\tau \to \tau_{re}$. Equation (2.19) holds when all the corresponding wavelengths are shorter than the Hubble radius (i.e. for $k\tau \gg 1$) and in the same approximation $G_k(\tau)$ becomes

$$G_k(\tau) = \frac{e^{-ik\tau_{ex}}}{a}\sqrt{\frac{k}{2}}\mathcal{Q}_k(\tau_{ex},\tau_{re})\left(\frac{a_{re}}{a_{ex}}\right)$$
$$\times\left\{\frac{\mathcal{H}_{re}}{k}\cos(k\Delta\tau) - \sin(k\Delta\tau)\right\}. \tag{2.20}$$

Equations (2.19) and (2.20) assume an expanding background (i.e. $a_{re} \gg a_{ex}$), but they are otherwise general since the rates at τ_{ex} and τ_{re} have not been specified. After inserting Eqs. (2.19) and (2.20) into Eq. (2.6) we obtain

$$\Omega_{gw}(k,\tau) = \frac{2k^4}{3\pi a^4 H^2 M_P^2}|\mathcal{Q}(\tau_{ex},\tau_{re})|^2\left(\frac{a_{re}}{a_{ex}}\right)^2\left(1 + \frac{\mathcal{H}_{re}^2}{k^2}\right)$$
$$\times\left[1 + \mathcal{O}\left(\frac{\mathcal{H}}{k}\right)\right]. \tag{2.21}$$

Equations (2.19)–(2.21) hold up to corrections $\mathcal{O}(\mathcal{H}/k)$ that are small for wavelengths shorter than the Hubble radius. As long as the relevant wavelengths appearing in Fig. 1 do their first crossing during the inflationary stage where $k\tau_{ex} = \mathcal{O}(1)$. It can happen however that $k\tau_{re} \ll 1$ if the second crossing takes place when $\epsilon(a) \to \mathcal{O}(2)$, i.e. close to a radiation-dominated stage of expansion. To understand this relevant limit we recall that Eq. (2.8) can also be written in a decoupled form:

$$f_k'' + \left[k^2 - \frac{a''}{a}\right]f_k = 0, \qquad g_k = f_k' - \mathcal{H} f_k, \tag{2.22}$$

where $f_k(\tau) = a(\tau)F_k(\tau)$ and $g_k(\tau) = a(\tau)G_k(\tau)$. In the language of Eq. (2.22) the solutions given in Eqs. (2.12), (2.19) and (2.20) hold, respectively, for $k^2 \ll |a''/a|$ and for $k^2 \gg |a''/a|$. The turning points where the analytical

behavior of the solution changes are defined by $k^2 \simeq |a''/a|$ that can also be rewritten as

$$k^2 = a^2H^2[2 - \epsilon(a)], \tag{2.23}$$

where, as before, $\epsilon(a) = -\dot{H}/H^2$ is the slow-roll parameter.[9] When $\epsilon \neq 2$ both turning points are regular and this means that the two solutions of Eq. (2.23) are in fact $k\tau_{ex} = \mathcal{O}(1)$ and $k\tau_{re} = \mathcal{O}(1)$. For instance when a given wavelength crosses the Hubble radius during inflation we have that $\epsilon \ll 1$ and $k \simeq a_{ex}H_{ex}$ that also means, by definition, $k\tau_{ex} \simeq 1$. Similarly if the given wavelength reenters in a decelerated stage of expansion different from radiation we also have that $k \simeq a_{re}H_{re}$. However, if the reentry occurs in the radiation stage (or close to it) we have that $\epsilon_{re} \to 2$ and the condition (2.23) implies that $k\tau_{re} \ll 1$. In Eq. (2.21) the two situations are distinct since $\mathcal{H}_{re}^2/k^2 = \mathcal{O}(1)$ when $\epsilon_{re} \neq 2$ while $\mathcal{H}_{re}^2/k^2 \gg 1$ for $\epsilon_{re} \to 2$. We shall get back to this point in Sec. III where Eq. (2.21) will be used to deduce the analytic form of the spectral slopes in the different frequency domains. For short wavelengths the mode function for the curvature inhomogeneities is given by

$$\overline{F}_k(\tau) = \frac{e^{-ik\tau_{ex}}}{z\sqrt{2k}}\overline{\mathcal{Q}}_k(\tau_{ex}, \tau_{re})\left(\frac{z_{re}}{z_{ex}}\right) \times \left\{\frac{\mathcal{F}_{re}}{k}\sin[k\Delta\tau] + \cos[k\Delta\tau]\right\}, \tag{2.24}$$

and if we now insert Eqs. (2.19) and (2.24) into Eq. (2.10) we obtain the wanted form of $r_T(k,\tau)$ valid for $\tau \geq \tau_{re}$ in the short-wavelength limit (i.e. for $k\tau > 1$):

$$r_T(k,\tau) = 8\ell_P^2\left[\frac{z(\tau)}{a(\tau)}\right]^2\left(\frac{a_{re}}{a_{ex}}\right)^2\left(\frac{z_{ex}}{z_{re}}\right)^2\mathcal{G}^2(k\Delta\tau),$$
$$\mathcal{G}(k\Delta\tau) = \frac{\mathcal{F}_{re}\sin(k\Delta\tau) + k\cos(k\Delta\tau)}{\mathcal{H}_{re}\sin(k\Delta\tau) + k\cos(k\Delta\tau)}. \tag{2.25}$$

In the limit $\epsilon_{re} \to 2$ we also have $\mathcal{H}_{re}/k \simeq \mathcal{F}_{re}/k \gg 1$ and, in this case, $\mathcal{G}(k\Delta\tau) \to 1$. Conversely, when $\epsilon_{re} \neq 2$ we have instead that $\mathcal{H}_{re}/k \simeq \mathcal{F}_{re}/k = \mathcal{O}(1)$; also in this situation $\mathcal{G}(k\Delta\tau) = \mathcal{O}(1)$. We can therefore deduce from Eq. (2.25) that

$$r_T(k,\tau) = 16\epsilon_k\frac{\epsilon(\tau)}{\epsilon_{re}}, \qquad \tau \geq \tau_{re}, \qquad k\tau > 1. \tag{2.26}$$

[9]While during inflation $\epsilon \ll 1$, in the postinflationary phase the background decelerates (but still expands) and $\epsilon(a) = \mathcal{O}(1)$.

It seems that, in practice, $\epsilon(\tau)$ is piecewise constant after inflation and it is of the order of ϵ_{re} so that $r_T(k,\tau) \to 16\epsilon_k$ even for short wavelengths. The constancy of $\epsilon(\tau)$ is more or less obvious when the background expands as simple power law but if the reentry of the wavelength takes place when the inflaton potential is still dominant (and oscillating) $\epsilon(\tau)$ is still approximately constant. For this purpose we can first write $\epsilon(\tau)$ in terms of the inflaton potential $V(\varphi)$, i.e.

$$\epsilon(\tau) = -\dot{H}/H^2 = 3\dot{\varphi}^2/(\dot{\varphi}^2 + 2V). \tag{2.27}$$

As suggested long ago the coherent oscillations of the inflaton imply the approximate constancy of the corresponding energy density[10] [43]; for immediate convenience the inflaton potential around its minimum can be parametrized as

$$V(\varphi) = V_0(\varphi/\overline{M}_P)^{2q}, \to \dot{\varphi} = \sqrt{2V_{\max}}\sqrt{1 - x^{2q}}, \tag{2.28}$$

where $x = \varphi/\varphi_{\max}$. If the numerator and the denominator of Eq. (2.27) are averaged over one period of oscillations (say between $\varphi = 0$ and $\varphi = \varphi_{\max}$) $\epsilon(\tau)$ becomes

$$\epsilon(\tau) = \frac{3\int_0^1\sqrt{1 - x^{2q}}dx}{\int_0^1 dx/\sqrt{1 - x^{2q}}} = \frac{3q}{q+1}. \tag{2.29}$$

Thus, from Eqs. (2.26) and (2.29), $\epsilon(\tau)/\epsilon_{re} \to 1$ when the reentry occurs during a phase driven by the coherent inflaton oscillations. With the same technique the average expansion rate during a phase of coherent oscillations follows from Eq. (2.29); in particular

$$\mathcal{H}' = \frac{1 - 2q}{q+1}\mathcal{H}^2 \Rightarrow a(\tau) = (\tau/\tau_1)^\delta,$$
$$\text{where } \delta = (q+1)/(2q-1). \tag{2.30}$$

This result implies that if the wavelengths exit during a stage dominated by the coherent oscillations of the inflaton we can expect that the slope of the spectral energy density can be determined according to Eq. (2.30). The evolution of the comoving horizon in Fig. 1 assumes a sequence of different expanding stages characterized by the constancy of the expansion rate. A fully equivalent strategy is to consider the continuous variation of δ implying

$$\frac{1}{\delta(\tau)} = -1 - \frac{1}{2}\frac{\partial\ln\rho_t}{\partial\ln a} = -1 + \epsilon(\tau), \tag{2.31}$$

[10]Indeed we have, in general, that $\dot{\rho}_\varphi + 3H\dot{\varphi}^2 = 0$ where $\rho_\varphi = \dot{\varphi}^2/2 + V$ is the energy density of the inflaton. However since $\dot{\rho}_\varphi \simeq 0$ and $3H\dot{\varphi}^2 \ll \dot{\rho}_\varphi$ we can also write that $\dot{\varphi}^2 = 2(V_{\max} - V)$ where $V_{\max} = V(\varphi_{\max})$.

where $\rho_t(a)$ denotes the total energy density governing the postinflationary evolution prior to radiation. In the case of inflaton-dominated oscillations $\rho_t(a) = \rho_\varphi$ and

$$\delta(a) = 1/[\epsilon(a) - 1] = (q+1)/(2q-1). \tag{2.32}$$

By going back to Fig. 1 we therefore have that when the given wavelength crosses the Hubble radius prior to radiation dominance the value of δ is scale dependent $\delta_k = \delta(\tau_{re}) = \delta(1/k)$. This relation follows by recalling that during the postinflationary stage illustrated in the cartoon of Fig. 1 $\delta(a) \neq 1$, which also implies $\epsilon(a) \neq 2$ in Eq. (2.23).

C. Consistency relations and some examples

In single-field scenarios the spectral index $n_s(k)$, the tensor-to-scalar ratio $r_T(k)$ and the tensor spectral index $n_T^{\rm low}(k)$ obey the consistency relations[11]

$$n_s(k) = 1 - 6\epsilon_k + 2\overline{\eta}_k, \qquad r_T(k) = 16\epsilon_k, \qquad n_T^{\rm low}(k) = -2\epsilon_k, \tag{2.33}$$

where $\epsilon_k = \epsilon(1/k)$ and $\overline{\eta}_k = \overline{\eta}(1/k)$ denote the slow-roll parameters evaluated when the bunch of wavelengths corresponding to the CMB scales exited the comoving horizon approximately N_k e-folds prior to the end of inflation. In more general terms it is well known that the slow-roll parameters are all time dependent (or field dependent) and they are defined, within the notations employed here, as

$$\epsilon = -\frac{\dot{H}}{H^2} = \frac{\overline{M}_P^2}{2}\left(\frac{V_{,\varphi}}{V}\right)^2, \qquad \eta = \frac{\ddot{\varphi}}{H\dot{\varphi}} = \epsilon - \overline{\eta}, \qquad \overline{\eta} = \overline{M}_P^2\left(\frac{V_{,\varphi\varphi}}{V}\right). \tag{2.34}$$

According to the current limits, the tensor-to-scalar ratio and the scalar spectral index are determined as [8–10]

$$r_T(k, \tau_{ex}) < \overline{r}_T, \qquad n_s(k, \tau_{ex}) = \overline{n}_s, \tag{2.35}$$

where $\overline{r}_T$ ranges between $\mathcal{O}(0.06)$ and $\mathcal{O}(0.03)$ while $0.96448 < \overline{n}_s < 0.96532$ with a central value corresponding to 0.9649. Once more, by definition, in Eq. (2.35) $r_T(k, \tau_{ex}) = r_T(k, 1/k) = r_T(k)$ and similarly $n_s(k, \tau_{ex}) = n_s(k, 1/k) = n_s(k)$. For the monomial potentials ϵ_k and $\overline{\eta}_k$ are of the same order and these scenarios are practically excluded by current data. We shall rather consider potentials with typical form given by

$$V(\Phi) = M^4 v(\Phi), \qquad \Phi = \varphi/\overline{M}_P, \tag{2.36}$$

where M denotes the energy scale of the potential. Inflation occurs for $\Phi \gg 1$ (and in this limit we therefore have $v(\Phi) \to 1$) while it ends for $\Phi \ll 1$. Using the parametrization of Eq. (2.36) the expressions of Eq. (2.34) get even simpler; for instance $\epsilon(\Phi) = (1/2)(v_{,\Phi}/v)^2$ and so on and so forth (see also the Sec. B 2 and the discussions therein). We can then write $v(\Phi)$ as the ratio of two functions scaling (approximately but not exactly) with the same power for $\Phi \gg 1$. An example along this direction is

$$v(\Phi) = \frac{\beta^p \Phi^{2q}}{[1 + \beta^2 \Phi^{\frac{4q}{p}}]^{\frac{p}{2}}}, \qquad 4q > p, \qquad \beta > 0. \tag{2.37}$$

In Eq. (2.37) β, p and q are the parameters of the potential and, for technical reasons, we consider the case $4q > p$. A q-dependent oscillating stage takes place for $\Phi \ll 1$ where the potential can be written as $v(\Phi) = \beta^p \Phi^{2q}$. By following the same strategy different concrete examples can be concocted like, for instance,

$$v(\Phi) = \frac{(e^{\gamma\Phi} - 1)^{2q}}{(e^{\frac{4\gamma q}{p}\Phi} + 1)^{\frac{p}{2}}}, \qquad 4q > p, \qquad \beta > 0. \tag{2.38}$$

While the examples along the lines of Eqs. (2.37) and (2.38) can be multiplied, for the present purposes, different functional forms of the potential do not radically modify the scaling of the slow-roll parameters and of the tensor-to-scalar ratio. To investigate this point it is interesting to compute $r_T(k)$ and $n_s(k)$ directly in terms of N_k and of the other parameters of the potential. For this purpose Eq. (2.33) must be evaluated when the wavelengths compatible with the pivot scale cross the Hubble radius during inflation (see Fig. 1). Thanks to the results of Appendix B [see in particular Eqs. (B16) and (B17)] $n_s(k)$ becomes

$$n_s(k) = n_s(N_k) = 1 - \frac{12 q^2 \beta^{-2/(1+2q/p)}}{[4q(p+2q)N_k/p]^{(p+4q)/(p+2q)}} - \frac{p+4q}{(p+2q)N_k}. \tag{2.39}$$

By always referring to Eqs. (B16) and (B17) the expressions of $r_T(k)$ and $n_T^{\rm low}(k)$ are given by

[11] In Eq. (2.33) $n_T^{\rm low}(k)$ denotes the low-frequency spectral index associated with the wavelengths reentering during the radiation stage. To avoid confusions we anticipate that in Sec. III one (or more) high-frequency spectral indices will also be introduced. The high-frequency spectral indices involve the wavelengths that reentered the effective horizon prior to radiation dominance, i.e. for $a < a_r$ in Fig. 1.

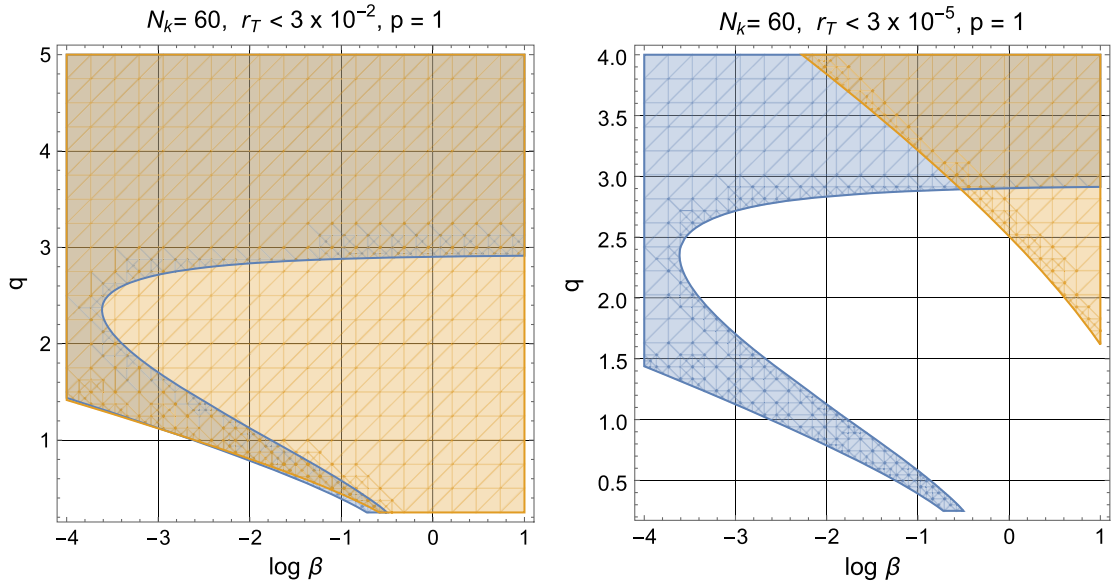

FIG. 2. If N_k is fixed, then Eqs. (2.39) and (2.40) together with the constraints of Eq. (2.35) define the allowed region of the parameter space which is illustrated here in the plane $(\log\beta, q)$. In the plot at the left we consider the overlap between the regions defined by $0.96448 < \overline{n}_s < 0.96532$ and by $r_T < 3\times 10^{-2}$. In the plot at the right the limit on $r_T(k)$ is reduced from $r_T < 3\times 10^{-2}$ to $r_T < 3\times 10^{-5}$. As the limit on $r_T(k)$ becomes more stringent the overlap shrinks and it is localized in the region of large q.

$$r_T(k) \equiv r_T(N_k) = \frac{32 q^2 \beta^{-2/(1+2q/p)}}{[4q(p+2q)N_k/p]^{(p+4q)/(p+2q)}},$$
$$n_T^{\rm low}(k) \equiv n_T^{\rm low}(N_k) = -\frac{4q^2\beta^{-2/(1+2q/p)}}{[4q(p+2q)N_k/p]^{(p+4q)/(p+2q)}}. \tag{2.40}$$

The results of Eqs. (2.39) and (2.40) are illustrated in Figs. 2–4 for different values of q, p and β. In Fig. 2 the overlap between the two regions defines the portion of the parameter space where the scalar spectral index is phenomenologically viable and the limit on $r_T(k)$ is safely enforced. By comparing the left and the right plots in Fig. 2 we see that the overlap shrinks as soon as the bounds on r_T become progressively more demanding. In the left plot of Fig. 2 the region bounded by a straight line and a curve follows by requiring that $n_s(k)$ falls within the 1σ observational limits set by the Planck collaboration complemented by the lensing observations, i.e. $\overline{n}_s = 0.9649 \pm 0.0042$. The addition of the baryon acoustic oscillations would imply a slightly different figure (i.e. $\overline{n}_s = 0.9665 \pm 0.0038$) which is however not essential for the illustrative purposes of this discussion. The second region bounded by a straight line in the left plot of Fig. 2 corresponds to the requirement $r_T < 0.03$. In the right plot the limit on r_T (i.e. $r_T < 3\times 10^{-5}$) defines the approximate triangular shape in the upper corner while the other shaded region coincides with the one of the left plot.

In Fig. 2 we fixed $p \to 1$ and $N_k = 60$ and this is consistent with the determinations of N_k discussed in Appendix A in the absence of any postinflationary stage of expansion deviating from the dominance of radiation. We shall get back to this choice at the end of Sec. IV and question its validity in the case of a long stage of postinflationary expansion slower than radiation. As the value of p increases this progressive reduction of the overlap already pointed out in Fig. 2 is further exacerbated and this conclusion follows from Fig. 3 where $p \to 3$. If we compare the right plots of Figs. 2 and 3 we see that the distance between the two nonoverlapping regions increases. Similarly if we compare the left plots of Figs. 2 and 3 we have that the overlap between the allowed regions is comparatively smaller for $p = 3$ than for $p = 1$. A final interesting observation is illustrated in Fig. 4 where we imposed $r_T < 3\times 10^{-5}$ for two different values of p. By looking at Fig. 3 the allowed regions looked completely absent; it happens, however, that for comparatively larger values of q the constraints on r_T and the requirements on n_s are concurrently satisfied.[12]

The same analysis leading to Figs. 2–4 can be repeated in the case of similar potentials like the one of Eq. (2.38). Using again the procedure outlined in Appendix B we can then deduce, for instance, that

$$n_s(k) \simeq 1 - \frac{3}{\gamma^2 N_k^2} - \frac{2}{N_k}, \qquad r_T(k) \simeq \frac{8}{\gamma^2 N_k^2},$$
$$n_T^{\rm low}(k) \simeq -\frac{1}{\gamma^2 N_k}. \tag{2.41}$$

[12]As already mentioned the results obtained so far, especially for the large q values, are only partially accurate. Indeed as we saw in Eq. (2.30) at the end of inflation the oscillatory regime for $q \gg 1$ implies that $0 < \delta < 1$. In this case the total number of e-folds may be larger than 60 and this correction may have a relevant impact as we shall see in Sec. IV.

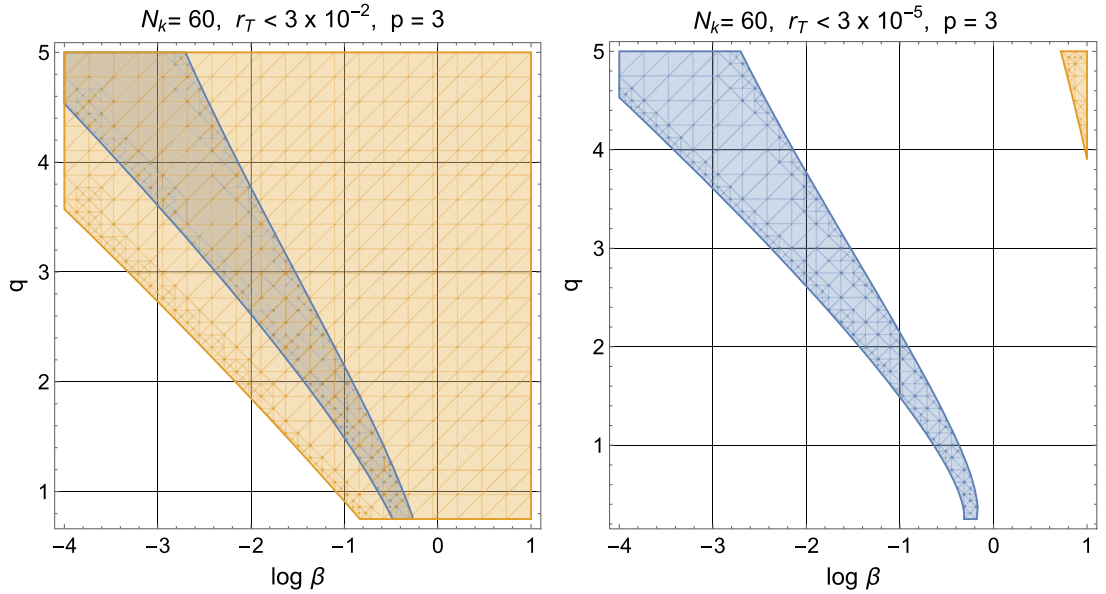

FIG. 3. The same logic of Fig. 2 can be illustrated for a larger value of the parameter p. In this case a reduction of 3 orders of magnitude of r_T (from 3×10^{-2} to 3×10^{-5}) implies that the overlap between the two regions completely disappears. This means that none of the parameters appearing in the right plot would be phenomenologically acceptable in case future limits would imply $r_T < 3 \times 10^{-5}$; this happens since in the central region of the plot the scalar spectral index is correctly reproduced but the tensor to scalar ratio is always larger than 3×10^{-5} and the two regions never overlap.

Equation (2.41) holds for $\Phi_k > 1$ and $N_k \gg 1$; in this limit, Eq. (2.41) reproduces in fact the result obtainable in the case of the potential

$$v(\Phi) = (1 - e^{-\beta\Phi})^{2q}, \qquad \beta > 0, \quad q > 0, \qquad (2.42)$$

where the analog of Eq. (2.41) is obtained by simply replacing $\gamma \to \beta$ (see, in this respect, the recent analysis of Ref. [44]). The main difference between the example of Eq. (2.33) and the examples of Eqs. (2.38) and (2.42) is the q dependence: while in the case of Eqs. (2.38) and (2.42)

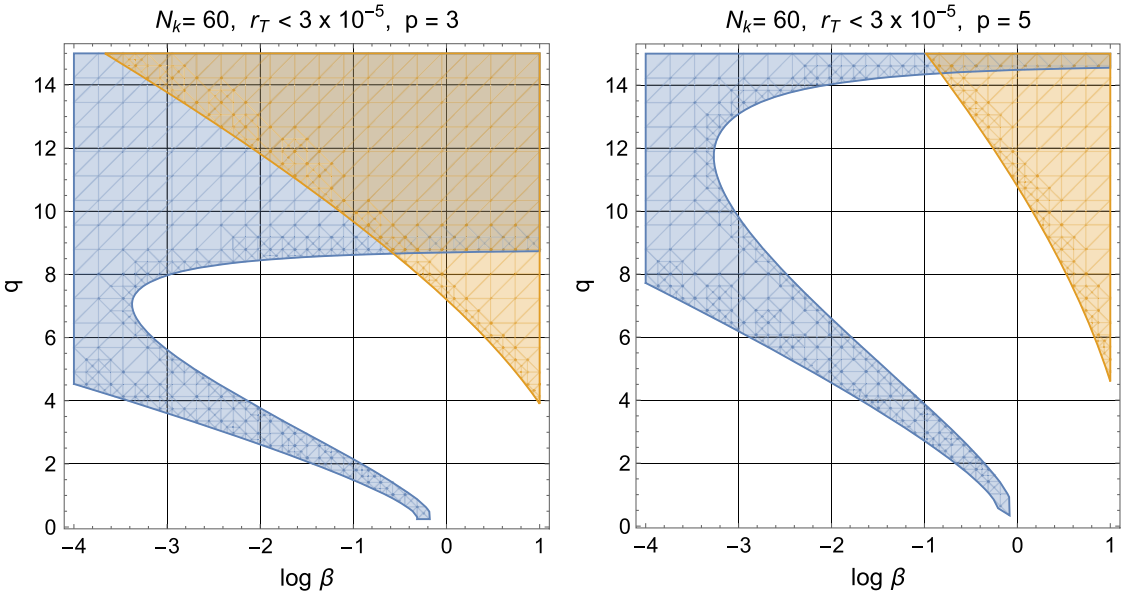

FIG. 4. In both plots of this figure we imposed $r_T < 3 \times 10^{-5}$ for two different values of p. The left plot of this figure coincides with the left plot of Fig. 3 but the range of q is larger. From both plots we see that the region where the constraints are simultaneously satisfied moves towards large q values. We can then recall from Eq. (2.30) that for $q \gg 1$ the inflaton oscillations effectively lead to a phase expanding at a rate that is slower than radiation (i.e. $\delta < 1$).

the spectral indices and the tensor-to-scalar ratio do not depend on q, Eqs. (2.39) and (2.40) show the opposite. The plateaulike potentials seem to imply a certain degree of fine-tuning that has been pointed out also at the level of the initial conditions of the inflaton. It is true that for generic initial conditions of φ at the beginning of inflation both the kinetic energy and the spatial gradients should be of the same order and both larger than the potential $V(\varphi) = \mathcal{O}(M^4)$. Since the kinetic energy of the inflaton redshifts faster than the spatial gradients, it can happen that inflation is prevented by the dominance of the spatial inhomogeneities, unless some amount of fine-tuning is invoked [45,46].

If $n_s(k)$ and $r_T(k)$ approximately follow from Eq. (2.41), then the tensor-to-scalar ratio cannot be excessively reduced by keeping the agreement of the scalar spectral index with the observational data. It is true that in the case of a long postinflationary stage N_k may be larger than $\mathcal{O}(60)$ but besides this possibility (separately analyzed in Sec. IV after the derivation of the lower bounds on r_T), a further reduction of $r_T(k)$ may occur either when the consistency relations are broken or for a different class of inflaton potentials. The consistency relations can be broken because of the protoinflationary dynamics [41,42] and they can also be modified because of the running associated with the scalar spectral index [47]; in both cases we could have that $r_T < 10^{-4}$. In the context of hilltop potentials r_T can be reduced [48] and it has even be argued that, in this framework, it is possible to construct models with parametrically small r_T [49]. These examples are constructed in terms of certain classes of fast-roll potentials where η [see Eq. (2.34)] is actually constant [50–52]. All these situations have a counterpart in the present framework but their impact will not be explicitly discussed here.

Before closing this section it is appropriate to remark that we consider here the situation where the potential reduction of the tensor to scalar ratio at the CMB scale follows, generally speaking, from a sequence of stages expanding either faster or slower than radiation as described in Fig. 1. In the past a single stage of prolonged reheating has been suggested to increase the values of r_T [53–55]. In this respect, from Eq. (2.1) [see also Eqs. (A7) and (A8)] an enhancement of r_T may occur when a long reheating phase follows the inflationary stage provided, after inflation, the background expands faster than radiation. In this instance N_k may become much smaller than $\mathcal{O}(60)$ so that the tensor to scalar ratio could increase and even reach the typical values $r_T = \mathcal{O}(0.2)$ initially motivated by the explanation of the BICEP2 data on the B-mode polarization [5]. A concurrent perspective was, at that time, the violation of the consistency relations caused, for instance, by the quantum initial conditions in the case of a relatively short inflationary stage [56]. Both viewpoints are unrelated with the one conveyed here for a twofold reasons. The BICEP2 measurements of Ref. [5] were in fact affected by serious foreground contaminations and are now superseded since the present bounds on r_T are much smaller, i.e. as already mentioned $r_T \leq 0.06$ or even $r_T < 0.03$ [8–10]. The second point is directly related to the main question of this paper which is, in short, the following: how small should r_T be in order to preserve a high-frequency signal even in the absence of a low-frequency detection? Although the authors do not present detailed analyses of the high-frequency spectrum, the results of the forthcoming sections imply that for the scenarios of Refs. [53–55] $h_0^2\Omega_{gw}(\nu, \tau_0)$ in the audio and MHz bands is even smaller than in the standard case. Indeed for a long postinflationary phase expanding faster than radiation the high-frequency spectrum sharply decreases without any intermediate maximum. On the contrary in the present analysis we seriously consider the possibility that the relic gravitons are invisible in the aHz region but potentially detectable in the audio and GHz bands: this perspective is just orthogonal to the one of Refs. [53–55].

For the above reasons the monomial potentials discussed in Refs. [53–55] differ from the ones of Eqs. (2.37) and (2.38) that are characterized by a flat plateau in the inflationary limit. In the present framework these potentials are just illustrative examples since what matters for the subsequent discussions is *not* the detailed shape of the potential but the general profile of the expansion rate; nonetheless Eqs. (2.37) and (2.38) describe the situation where $v(\Phi)$ is nearly flat for $\Phi \gg 1$ while they go as a power near the origin. Potentials with different analytical forms (but with similar properties) have been studied in Ref. [57] (see also [58]); in this framework gravitational waves can be used to break some inflationary degeneracies. The spectral energy density computed in Refs. [57,58] follows however from the general analyses of Refs. [20,21,34,59] where the idea was to normalise the low-frequency spectrum at the highest value of r_T compatible with the observations.[13] In this paper, on the contrary, we shall allow r_T to be smaller (or even much smaller) than the current phenomenological bounds. Last but not least Ref. [60] draws a number of conclusions on the interplay between low-frequency determinations and high-frequency measurements in the audio band. Although these claims are overall reasonable, Ref. [60] assumes a single spectral slope between the aHz and the audio band. This is just the conventional perspective where all the $\delta_i \to 1$ in Fig. 1. The viewpoint of this paper is instead that, above the curvature scale of the nucleosynthesis, the expansion rate can only be tested via the relic graviton backgrounds and the measurements of the spectral energy density in the audio and MHz bands can be ultimately viewed as direct probes of the early expansion history. Furthermore, as it will be clear from the two subsequent sections, *any* deviation from radiation

[13]Note, incidentally, that various sources of suppression at intermediate frequencies (like the free streaming of the neutrinos) have not been included in Ref. [58].

dominance involves a further spectral slope so that it would be incorrect to modify the postinflationary evolution without taking into account that also the slopes of the spectral energy density are correspondingly modified. For these reasons the arguments of Ref. [60] seem only marginally relevant in the present framework.

III. THE SPIKES OF THE SPECTRAL DENSITY

Instead of scanning the range of $r_T(k)$ and of the postinflationary expansion rates of Fig. 1 it seems more plausible to identify preliminarily all the physical situations where the spectral energy density exceeds the predictions of the concordance scenario for frequencies larger than $\mathcal{O}(10^{-2})$ nHz. From the phenomenological constraints we can argue that the most stringent limits are obtained when $h_0^2\Omega_{gw}(\nu,\tau_0)$ develops a maximum either in the high-frequency region (i.e. approximately between few MHz and the GHz) or in the audio band. A further spike in the nHz range could only develop if $h_0^2\Omega_{gw}(\nu,\tau_0)$ sharply increases between $\mathcal{O}(10^{-2})$ nHz and few nHz; this frequency range is however too narrow for an appreciable growth of the spectral energy density.[14]

A. Spikes in the ultra-high-frequency region

The presence of a broad spike in the high-frequency domain implies that the profile of the comoving horizon of Fig. 1 consists of a unique postinflationary stage extending between H_1 and H_r: only in this case we could have a single frequency domain where the spectral energy density always increases up to the GHz range. In this class of scenarios (illustrated in Fig. 5) $h_0^2\Omega_{gw}(\nu,\tau_0)$ comprises two separated frequency regions: a quasiflat plateau (typically arising for $\nu<\nu_r$) and a high-frequency hump approximately corresponding to $\nu=\mathcal{O}(\nu_{\rm max})$. From the considerations developed in Eqs. (A15)–(A18) $\nu_{\rm max}$ and ν_r can be estimated as follows:

$$\nu_{\rm max}=\xi^{\frac{\delta-1}{2(\delta+1)}}\overline{\nu}_{\rm max},\qquad \nu_r=\sqrt{\xi}\overline{\nu}_{\rm max},\qquad \xi=H_r/H_1. \tag{3.1}$$

Besides $\nu_{\rm max}$ and ν_r there is also a more conventional third frequency region for $\nu<\nu_{eq}$. In this domain, the corresponding wavelengths exited the comoving horizon during the early stages of inflation and reentered after matter-radiation equality; this bunch of wavelengths is slightly larger than the shaded stripe illustrated in Fig. 1. The equality frequency ν_{eq} is given by

$$\nu_{eq}=\frac{k_{\rm eq}}{2\pi}=1.597\times10^{-17}\left(\frac{h_0^2\Omega_{M0}}{0.1411}\right)\left(\frac{h_0^2\Omega_{R0}}{4.15\times10^{-5}}\right)^{-1/2}\ {\rm Hz}, \tag{3.2}$$

where $k_{eq}=0.0732h_0^2\Omega_{M0}\ {\rm Mpc}^{-1}$ and, as usual, Ω_{M0} is the present fraction in dusty matter.

The slopes of $h_0^2\Omega_{gw}(\nu,\tau_0)$ in the different frequency regions follow from Eq. (2.21). For the wavelengths that exited the Hubble radius during inflation and reentered in the radiation stage we have that the structure of the turning point is singular [i.e. $\epsilon(\tau_{re})\to2$]; this means that, thanks to Eq. (2.23),

$$k\simeq a_{ex}H_{ex}\simeq-\frac{1}{(1-\epsilon_k)\tau_{ex}},\qquad k\tau_{re}\ll1. \tag{3.3}$$

Because of Eq. (3.3) the term $\mathcal{H}_{re}/k\gg1$ dominates in Eq. (2.21) and $\Omega_{gw}(\nu,\tau)\propto(\nu/\nu_r)^{n_T^{\rm low}}$ for $\nu<\nu_r$. If the wavelengths reenter instead before radiation was dominant [and when the background approximately expands as $a(\tau)\simeq(\tau/\tau_1)^\delta$ with $\delta\neq1$] for $\nu_r<\nu<\nu_{\rm max}$ we have that $\Omega_{gw}(\nu,\tau)\propto(\nu/\nu_r)^{n_T^{\rm high}}$, where $n_T^{\rm high}$ is the high-frequency spectral index. The explicit expressions of $n_T^{\rm low}$ and $n_T^{\rm high}$ are given by

$$n_T^{\rm low}=-2\epsilon_k,\qquad n_T^{\rm high}=\frac{2-4\epsilon_k}{1-\epsilon_k}-2\delta. \tag{3.4}$$

If the consistency relations are enforced the $n_T^{\rm high}$ can also be expressed as

$$n_T^{\rm high}(r_T,\delta_k)=\frac{32-4r_T}{16-r_T}-2\delta=2(1-\delta)+\mathcal{O}(r_T),\qquad r_T=r_T(k). \tag{3.5}$$

The high-frequency spectral index of Eq. (3.5) depends both on r_T and δ; however, as long as $r_T\ll\mathcal{O}(10^{-2})$ the corrections induced by the finite value of r_T can be safely neglected. For the sake of conciseness we shall be using the stenographic notation $r_T(k)=r_T$ where it is understood that $k=\mathcal{O}(k_p)$ and the corresponding scales are the CMB wavelengths. The spectral energy density induced by a modified postinflationary history bears the mark of the evolution of the comoving horizon of Fig. 1 [61]. In particular, when the post-inflationary expansion rate is *slower* than radiation $\delta<1$ the high-frequency spectral index is positive and $h_0^2\Omega_{gw}(\nu,\tau_0)$ is comparatively larger than in the case $\delta>1$ where the background expands faster than radiation.[15] The case $\delta<1$ has been analyzed long ago

[14] For the sake of conciseness the nHz region is not be explicitly treated in this section but the corresponding constraints are anyway analyzed at the end of Sec. IV.

[15] When $\delta>1$ the high-frequency spectral index of Eq. (3.5) gets negative: in this case there are, in practice, no further constraints besides the low-frequency limits that translate into the upper bound on r_T. This means that at high frequencies $h_0^2\Omega_{gw}(\nu,\tau_0)$ always decreases as a function of ν and the maximal frequency of the spectrum is much smaller than $\mathcal{O}(100)$ MHz.

[20] (see also [21,22]) and a particular realization is provided by a stage dominated by the kinetic term of the inflaton-quintessence field [62] (see also [63,64]). The enhancement of the spectral energy density occurring when the background expand slower than radiation arises in a number of apparently different contexts (see e.g. [65–67]) that reproduce however the same basic dynamical situation of Refs. [20–22] where the inflationary phase is followed by a stiff stage of expansion. If the postinflationary evolution is dominated by the inflaton oscillations, then the averaged evolution of the comoving horizon may mimic the timeline of a stiff epoch [43,59]. Recalling the results of Eqs. (2.29)–(2.31) we have that the averaged expansion of the background is slower than radiation provided $q > 2$ assuming the shape of the potential is the one of Eq. (2.29). It is relevant to mention, in this respect, that the techniques of Ref. [59] can be used to compute the high-frequency slope before and after the averaging suggested in Ref. [43]. It turns out that, in both situations, the high-frequency spectral slope is exactly the same.

In Fig. 5 the three curves illustrate the spectral energy density in critical units for different sets of parameters that have been chosen, in short, as follows: (i) for the full curve (labeled by $r_T = 0.03$) the high-frequency spectral index is $n_T^{\rm high} = 0.62$ and the related ξ is $\xi = 10^{-28}$; (ii) the dashed curve corresponds to $r_T = 3 \times 10^{-4}$ while $n_T^{\rm high}$ and ξ are, respectively, 0.8 and 10^{-30}; (iii) for the dot-dashed spectrum we have $r_T = 3 \times 10^{-6}$, $n_T^{\rm high} = 0.9$ and always $\xi = 10^{-30}$.

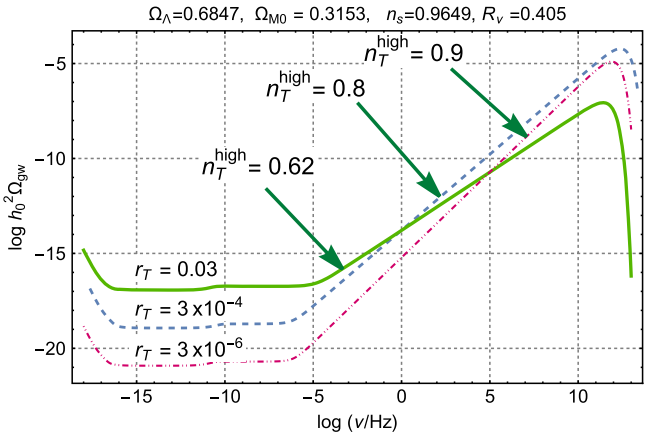

FIG. 5. For three different choices of the tensor to scalar ratio $h_0^2\Omega_{gw}(\nu, \tau_0)$ is illustrated as a function of the comoving frequency; common logarithms are employed on both axes. The high-frequency spectral indices have been chosen with the purpose of demonstrating that lower values of r_T do not necessarily imply a smaller signal at high frequencies. On the contrary, even though in all the examples we assumed that the consistency relations are enforced, the late-time parameters correspond to the fiducial values of the concordance paradigm. At low frequencies all the most relevant sources of suppression have been taken into account and, in particular, the free streaming of neutrinos.

Except for the full line of Fig. 5, the remaining two spectra correspond to much lower values of r_T. However, as we can see, in spite of a reduction of r_T the signal in the ultra-high-frequency region remains quite large and it must be constrained by the big bang nucleosynthesis bound [31–33] as well as by the direct limits of wideband interferometers (see in particular [25,26,39] for a review).

A reduction of r_T does not necessarily entail a suppression of the signal in the in MHz and GHz bands. On the contrary, if we look at the dot-dashed curve in Fig. 5 (corresponding to $r_T = 3 \times 10^{-6}$) the maximal value of $h_0^2\Omega_{gw}(\nu_{\rm max}, \tau_0)$ in this case is larger than for $r_T = 0.03$ (full curve in Fig. 5). As we shall see more specifically in Sec. IV the dashed and the dot-dashed curves in Fig. 5 are actually excluded by the nucleosynthesis bound and this shows, once more, that the limits on the high-frequency spike translate indirectly into a constraint on r_T. It actually happens that larger values of r_T are less constrained than the lower ones and, from a purely qualitative viewpoint, the examples of Fig. 5 may even suggest that, when the values of r_T are too small, the amplitude of the high-frequency spike is even more restricted.

As the values of the tensor-to-scalar ratio get progressively reduced the accurate determination of the low-frequency plateau of Fig. 5 becomes more essential and they are not only determined by r_T but also by the neutrino free streaming that suppresses $h_0^2\Omega_{gw}(\nu, \tau_0)$ for $\nu < \nu_{bbn}$ [68–72] where ν_{bbn} is the frequency corresponding to the big bang nucleosynthesis:

$$\nu_{bbn} = 2.3 \times 10^{-2} \left(\frac{g_\rho}{10.75}\right)^{1/4} \left(\frac{T_{bbn}}{\rm MeV}\right) \times \left(\frac{h_0^2\Omega_{R0}}{4.15 \times 10^{-5}}\right)^{1/4} {\rm nHz}. \tag{3.6}$$

The spectra of Fig. 5 correspond to the fiducial parameters the last Planck data release and the simplest possibility has been considered namely the case of three massless neutrinos where $R_\nu = \rho_\nu/(\rho_\gamma + \rho_\nu) = 0.405$, as indicated on top of each plots [8–10]. In Eq. (3.6) g_ρ is the effective number of relativistic species associated with the energy density.[16]

To make sure that radiation sets in before big bang nucleosynthesis the condition $\xi \geq 10^{-38}$ should be imposed [see also the discussion prior to Eq. (A5)]; but we can already see from Fig. 5 that the combined effect of a reduction of r_T and of an increase of $n_T^{\rm high}$ for a sufficiently small value of ξ [e.g. $\xi = \mathcal{O}(10^{-30})$] may be incompatible

[16]Other sources of suppression (taken into account in Fig. 5 and in the remaining plots) include the late-time dominance of dark energy and the evolution of relativistic species (see e.g. [39] for a review).

with the limits on the relativistic species at the nucleosynthesis time requiring

$$h_0^2 \int_{\nu_{bbn}}^{\nu_{\rm max}} \Omega_{gw}(\nu,\tau_0) d\ln\nu < 5.61\times 10^{-6} \left(\frac{h_0^2\Omega_{\gamma 0}}{2.47\times 10^{-5}}\right) \Delta N_\nu, \tag{3.7}$$

where $\Omega_{\gamma 0}$ is the (present) critical fraction of CMB photons. Equation (3.7) sets an indirect constraint on the extrarelativistic species possibly present at the time of nucleosynthesis. Since Eq. (3.7) is also relevant in the context of neutrino physics for historic reasons the limit is expressed in terms of ΔN_ν (i.e. the contribution of supplementary neutrino species). The actual bounds on ΔN_ν range from $\Delta N_\nu \leq 0.2$ to $\Delta N_\nu \leq 1$ so that the integrated spectral density in Eq. (3.7) must range, at most, between 10^{-6} and 10^{-5}. For the present purposes it is also useful to mention that the numerical results of Fig. 5 can be parametrized as

$$h_0^2\Omega_{gw}(\nu,\tau_0) = \mathcal{N}_\rho r_T \left(\frac{\nu}{\nu_p}\right)^{n_T^{\rm low}} \mathcal{T}^2_{\rm low}(\nu/\nu_{eq}) \mathcal{T}^2_{\rm high}(\nu/\nu_r,\delta), \tag{3.8}$$

where $\mathcal{N}_\rho = 4.165\times 10^{-15}$ for $h_0^2\Omega_{R0} = 4.15\times 10^{-5}$ and $\nu_p = k_p/(2\pi) = 3.092$ aHz. In Eq. (3.8) $\mathcal{T}^2_{\rm low}(\nu/\nu_{eq})$ and $\mathcal{T}^2_{\rm high}(\nu/\nu_r,\delta)$ denote, respectively, the low-frequency transfer function and its high-frequency counterpart. Both transfer functions are directly computed in terms of the spectral energy density [34] (see also [59]), not for the spectral amplitude.[17] The expression of $\mathcal{T}_{\rm low}(\nu/\nu_{eq})$ is

$$\mathcal{T}_{\rm low}(\nu/\nu_{eq}) = \sqrt{1 + c_2\left(\frac{\nu_{eq}}{\nu}\right) + b_2\left(\frac{\nu_{eq}}{\nu}\right)^2}, \qquad c_{eq} = 0.5238, \qquad b_{eq} = 0.3537. \tag{3.9}$$

Unlike $\mathcal{T}_{\rm low}(\nu/\nu_{eq})$, the high-frequency transfer function $\mathcal{T}_{\rm high}(\nu/\nu_r,\delta)$ depends on the value of δ so that it does not have a general form. However, as long as $\nu > \nu_r$, the high-energy transfer function can be approximated as $\mathcal{T}^2_{\rm high} \to (\nu/\nu_r)^{n_T^{\rm high}}$ so that the full spectral energy density at high frequency becomes, in this case,

$$h_0^2\Omega_{gw}(\nu,\tau_0) = \mathcal{N}_\rho r_T \left(\frac{\nu}{\nu_p}\right)^{n_T^{\rm low}} \mathcal{T}^2_{\rm low}(\nu_r/\nu_{eq}) \left(\frac{\nu}{\nu_r}\right)^{n_T^{\rm high}}, \qquad \nu_r \leq \nu \leq \nu_{\rm max}. \tag{3.10}$$

Equation (3.10) rests on the observation that $\mathcal{T}_{\rm low}(\nu_r/\nu_{eq}) \to 1$ for $\nu \geq \nu_r$; in the same limit it is also true that $n_T^{\rm low} = -r_T/8 \ll 1$ and, in this situation, the prefactor is practically frequency independent so that we can write

$$h_0^2\Omega_{gw}(\nu,\tau_0) = \overline{\mathcal{N}}_\rho(r_T,\nu) \left(\frac{\nu}{\nu_r}\right)^{n_T^{\rm high}}, \qquad \nu > \nu_r, \tag{3.11}$$

where $\overline{\mathcal{N}}_\rho(r_T,\nu)$ is now defined as

$$\overline{\mathcal{N}}_\rho(r_T,\nu) = \mathcal{N}_\rho r_T \left(\frac{\nu}{\nu_p}\right)^{n_T^{\rm low}} \mathcal{T}^2_{\rm low}(\nu_r/\nu_{eq}), \qquad n_T^{\rm low} = -r_T/8 \ll 1. \tag{3.12}$$

As before we can remark that, as long as $r_T < \mathcal{O}(10^{-2})$, $\partial\ln\overline{\mathcal{N}}_\rho/\partial\ln\nu \ll 1$ with a residual (mild) frequency dependence coming from neutrino free streaming. For simplified analytic estimates this dependence can be however ignored, at least in the first approximation. For instance, along this perspective we can estimate $\overline{\mathcal{N}}_\rho$ between $\mathcal{O}(10^{-16})$ and $\mathcal{O}(10^{-17})$.

B. The spectral energy density at the maximum

The spectral energy density can be estimated for $\nu = \mathcal{O}(\nu_{\rm max})$ by observing that the maximal frequency of the corresponds to the production of a single graviton pair (see [75] and discussion therein). If we introduce the mean number of produced graviton pairs per in each mode of the field [denoted hereunder by $\overline{n}(\nu,\tau_0)$], then the spectral energy density in critical units becomes

$$\lim_{\nu\to\nu_{\rm max}} \Omega_{gw}(\nu,\tau_0) \to \frac{128\pi^2}{3} \frac{\nu_{\rm max}^4}{H_0^2 M_P^2} \overline{n}(\nu_{\rm max},\tau_0). \tag{3.13}$$

By definition for $\nu \to \nu_{\rm max}$ we have that $\overline{n}(\nu_{\rm max},\tau_0) = \mathcal{O}(1)$. Recalling Eq. (3.1) and the expressions derived in the appendix A [see e.g. Eqs. (A11) and (A12) and discussion thereafter], Eq. (3.13) becomes

$$\Omega_{gw}(\nu_{\rm max},\tau_0) = \frac{8}{3\pi}\Omega_{R0} \left(\frac{H_1}{M_P}\right)^{4/(\delta+1)} \left(\frac{H_r}{M_P}\right)^{2(\delta-1)/(\delta+1)}. \tag{3.14}$$

Equation (3.14) holds in the case of a single postinflationary phase but it can be generalized to include all the relevant physical cases corresponding to the timeline of Fig. 1. The result of Eq. (3.14) slightly overestimates the

[17] In general the transfer function for the spectral energy density does not coincide with the transfer function computed for the spectral amplitude [59]; it is obtained by integrating numerically the mode functions across the radiation-matter transition for each k mode and by computing $\Omega_{gw}(\nu,\tau)$ for different frequencies. The advantage of the transfer function for the energy density is that while $\Omega_{gw}(\nu,\tau)$ is a mildly oscillating function of $k\tau$, the spectral amplitude exhibits larger oscillations that need to be averaged, as originally suggested in [73,74].

actual amplitude of the spectral energy density since it does not take into account the late-time sources of suppression related, for instance, with the neutrino free streaming. By now recalling the considerations of Appendix B [and, in particular, Eq. (B6)] we can trade H_1 for H_k and use that $(H_k/M_P) \simeq \sqrt{\pi \epsilon_k \mathcal{A}_{\mathcal{R}}}$. If we now impose the consistency relations we see that the maximum of the spectral energy density also depends on r_T.

C. Spikes in the audio band

As discussed in the previous subsections, when a single postinflationary stage precedes the radiation epoch $h_0^2 \Omega_{gw}(\nu, \tau_0)$ consists of three separate branches. However the spectral energy density may include multiple frequency domains [61] and, in this situation, a maximum may develop in the audio band. Besides the standard aHz region (i.e. $\nu_p < \nu < \nu_{eq}$) and part of the intermediate branch (for $\nu_{eq} < \nu < \nu_r$), the slopes in the two supplementary ranges (i.e. $\nu_r < \nu < \nu_2$ and $\nu_2 < \nu < \nu_{\rm max}$) depend on the values of the expansion rates in that region (i.e. δ_1 and δ_2). The different typical frequencies of this case are discussed in Appendix A [see, in particular, Eqs. (A15) and (A16)] and here the focus will be on the aspects that are directly relevant for the derivation of a bound on r_T.

Three different examples have been illustrated in Fig. 6 and the selected values of r_T reproduce the ones appearing in Fig. 5. With a unified notation the spectral slopes (denoted in Fig. 6 by $n_1^{\rm high}$ and $n_2^{\rm high}$) are

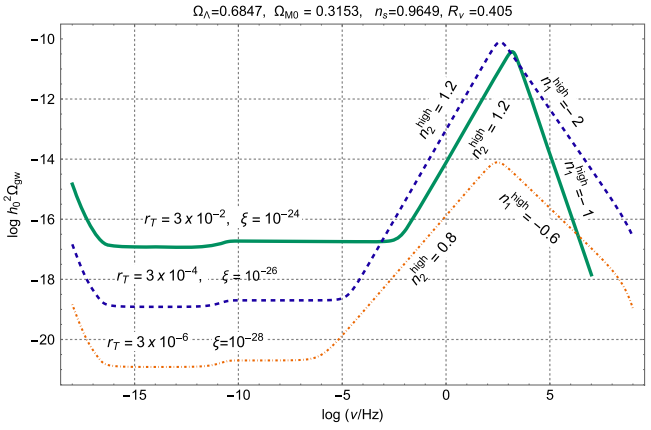

FIG. 6. The spectral energy density is illustrated with the same notations of Fig. 5. The values of r_T selected in this plot purposely match the ones of Fig. 5 but, in the present situation, the spike of $h_0^2 \Omega_{gw}(\nu, \tau_0)$ falls in the audio band. The various parameters have been selected by requiring that ν_2 (i.e. the frequency of the spike) is such that $\nu_2 = \mathcal{O}(\nu_{\rm audio})$. This is one of the most constraining cases since the direct bounds of wideband detectors fall into the audio band [23–26] (see also the discussion of Sec. IV). Note that the maximum corresponds to frequencies $\nu = \mathcal{O}(\nu_2)$ and not to $\nu_{\rm max}$. Typical frequencies $\nu = \mathcal{O}(\nu_{\rm max})$ are barely visible in rightmost region of the plot (see, in particular, the final part of the dot-dashed curve).

$$n_i^{\rm high} = \frac{32 - 4 r_T}{16 - r_T} - 2\delta_i, \qquad r_T \ll 1, \quad i = 1, 2. \tag{3.15}$$

The spectral energy density of Fig. 6 follows from the general evolution of the comoving horizon of Fig. 1 for $n = 3$ [see also Eqs. (A15) and (A16)] and this means that the postinflationary evolution (prior to radiation dominance) consists of two successive stages where the background first expands faster than radiation (i.e. $\delta_1 > 1$) and then slows down (i.e. $\delta_2 < 1$). According to the general arguments of Ref. [20] we have from Eq. (3.15) that the spectral energy density decreases for $\nu > \nu_2$ (i.e. $n_1^{\rm high} < 0$) while it increases at lower frequencies (i.e. $n_2^{\rm high} > 0$ for $\nu < \nu_2$). If $r_T \ll 0.03$ [8–10], then we have, in practice, that Eq. (3.15) reduces to

$$n_i^{\rm high} = 2(1 - \delta_k^{(i)}) + \mathcal{O}(r_T), \quad i = 1, 2. \tag{3.16}$$

The result of Eq. (3.16) follows directly from the expression of $\Omega_{gw}(\nu, \tau_0)$ given in Eq. (2.21) with the caveat that the comoving wavelengths reentering between a_1 and a_2 in Fig. 1 (and controlling the frequencies $\nu > \nu_2$) obey $k\tau_{re} = \mathcal{O}(1)$ and not $k\tau_{re} \ll 1$ as in the case of the wavelengths doing their second crossing during the radiation stage of expansion. In this case the spectral slopes are given by Eq. (3.16) and, in particular, $n_1^{\rm high} = 2(1 - \delta_1) < 0$ for the wavelengths reentering before a_2. Conversely for the wavelengths reentering between a_2 and a_r we have $n_2^{\rm high} = 2(1 - \delta_2) > 0$. If the timeline is reversed (and $\delta_1 < 1$ while $\delta_2 > 2$), then, instead of a spike, $h_0^2 \Omega_{gw}(\nu, \tau_0)$ exhibits a trough but this timeline would be comparatively less constrained than the one of Fig. 6.

All in all the two high-frequency branches of the spectral energy density can be parametrized as

$$h_0^2 \Omega(\nu, \tau_0) = \overline{\mathcal{N}}_\rho(r_T, \nu) \left(\frac{\nu}{\nu_r}\right)^{n_2^{\rm high}}, \qquad \nu_r < \nu < \nu_2, \tag{3.17}$$

$$h_0^2 \Omega(\nu, \tau_0) = \overline{\mathcal{N}}_\rho(r_T, \nu) \left(\frac{\nu_2}{\nu_r}\right)^{n_2^{\rm high}} \left(\frac{\nu}{\nu_2}\right)^{-|n_1^{\rm high}|}, \qquad \nu_2 < \nu < \nu_{\rm max}, \tag{3.18}$$

where we are implicitly assuming that $n_1^{\rm high} < 0$ and $n_2^{\rm high} > 0$ and $\overline{\mathcal{N}}_\rho(r_T, \nu)$ has been already defined in Eq. (3.12). The spectral energy density given of Eqs. (3.17) and (3.18) exhibits a maximum for $\nu = \mathcal{O}(\nu_2)$ but when $\delta_1 \to 1$ the maximum is replaced by a plateau since $h_0^2 \Omega_{gw}(\nu, \tau_0)$ flattens out (i.e. $n_1^{\rm high} \to 0$ for $\nu > \nu_2$) [61]. We then illustrated the situations that are phenomenologically more constraining; on this basis it is now possible to derive the lower bounds on r_T.

IV. LOWER BOUNDS ON r_T

We established that even if r_T controls the overall normalization of the spectral energy density, the tensor-to-scalar ratio also enters the typical frequencies of the spectrum through $\overline{\nu}_{\rm max}$ and ξ [see Eqs. (A11) and (A12) and discussions thereafter]; for this reason the position and the amplitudes of the spikes of $h_0^2\Omega_{gw}(\nu,\tau_0)$ are affected both by the postinflationary evolution and by r_T. If the background expands faster than radiation the maximal frequency may well shift from the MHz region to the audio band; conversely if the expansion rate is slower than radiation $\nu_{\rm max}$ may easily reach the GHz region. To stress this point we note that, if the consistency relations are enforced, then Eq. (3.14) can be written as[18]

$$h_0^2\Omega_{gw}(\nu_{\rm max},\tau_0) = \mathcal{C}(\delta) h_0^2\Omega_{R0}(r_T\mathcal{A}_{\mathcal{R}})^{2/(\delta+1)}\left(\frac{H_r}{M_P}\right)^{2(\delta-1)/(\delta+1)} \propto r_T^{2/(\delta+1)}. \tag{4.1}$$

In the second relation of Eq. (4.1) all the factors have been neglected except for the overall dependence on r_T and, by looking at this result, it could be argued that any suppression of r_T also reduces the high-frequency spike of the spectral energy density (see also Fig. 5 and discussions therein). However a reduction of r_T does not necessarily entail a suppression of the maximum of the spectral energy density since H_r, δ and r_T come from different physical considerations and are therefore independently assigned.

Let us first examine the case where, prior to radiation, the postinflationary evolution consists of a single stage expanding at a rate that is slower than radiation (i.e. $\delta < 1$). This case is illustrated in Fig. 5 and $h_0^2\Omega_{gw}(\nu,\tau_0)$ sharply increases below $\nu_{\rm max}$ but Eq. (4.1) also suggests that a suppression of few orders of magnitudes in r_T may be compensated by an increase of the overall normalization that contains (H_r/M_P). More specifically, when $H_r/M_P \ll 1$ and $\delta < 1$ the term $(H_r/M_P)^{2(\delta-1)/(\delta+1)}$ appearing in Eq. (4.1) overwhelms the reduction provided by $r_T^{2/(\delta+1)}$ unless r_T is really too small. If $\overline{\nu}_{\rm max} = \mathcal{O}(270)$ MeV for a pivotal value of the tensor-to-scalar ratio, then a reduction of r_T by 4 orders of magnitude only shifts $\overline{\nu}_{\rm max} \to \mathcal{O}(27)$ MHz. This is therefore a minor effect if compared with the modifications of the postinflationary evolution. Finally r_T also impacts the high-frequency slopes of the spectral energy density but this effect is negligible: we may consider, in this respect Eqs. (3.5) and (3.15) where the corrections induced on the spectral slopes are insignificant as long as $r_T < \mathcal{O}(10^{-2})$.

[18]The numerical factor $\mathcal{C}(\delta) = (1/6)(16/\pi)^{(\delta-1)/(\delta+1)}$ appearing in Eq. (4.1) does not alter the scaling properties of $\Omega_{gw}(\nu,\tau_0)$ for different values of r_T.

Even though, taken singularly, the different effects are easily estimated, the overall result of concurrent modifications of r_T and of the other parameters is not obvious and this is why we now present a numerical determination of $r_T^{\rm min}$, i.e. the minimal value of r_T compatible with the potential presence of a high-frequency spike. By definition for $r_T > r_T^{\rm min}$ the spectral energy density is larger than in the concordance scenario for the same value of r_T. This means that in the audio band and in the high-frequency domain the signal could be potentially detected by future instruments. Conversely for $r_T \leq r_T^{\rm min}$ the relic gravitons are invisible both in the aHz domain and also at higher frequencies.

A first necessary requirement for the estimate of $r_T^{\rm min}$ is that the frequency corresponding to radiation dominance must always exceed ν_{bbn} already introduced in Eq. (3.6):

$$\nu_r = \sqrt{\xi}\overline{\nu}_{\rm max} > \nu_{bbn}, \qquad \xi = H_r/H_1. \tag{4.2}$$

In the case of a single postinflationary phase $\xi = H_r/H_1$ whereas in the presence of multiple post-inflationary phases ξ is given by the product of the individual ξ_i [see, in this respect, Eqs. (A17) and (A18) and the discussion thereafter]. For a maximum in the audio band (see Fig. 6) we have $\xi = \xi_1\xi_2$ where $\xi_1 = H_2/H_1$ and $\xi_2 = H_r/H_2$. Equation (4.2) applies both for of a single maximum and in the case of multiple spikes but in the two situations the overall expression of ξ is different. Using together Eqs. (A12) and (4.2) we can also deduce the following bound on H_r/M_P:

$$\sqrt{H_r/M_P} \geq \frac{k_{bbn}}{(2\Omega_{R0})^{1/4}}(H_0M_P)^{-1/2}\mathcal{C}(g_s,g_\rho), \tag{4.3}$$

where, by definition, $k_{bbn} = 2\pi\nu_{bbn}$. If the explicit values of the various terms are inserted into Eq. (4.3) we may obtain that $\sqrt{H_r/M_P} \geq 1.95\times10^{-22}/\mathcal{C}(g_s,g_\rho)$ for $h_0^2\Omega_{R0} = 4.15\times10^{-5}$. The interesting point to stress, in this respect, is that while $\overline{\nu}_{\rm max}$ and ξ individually depend upon r_T, the bound of Eq. (4.2) does not depend on the tensor-to-scalar ratio. Indeed we have that while ξ scales as $r_T^{-1/4}$, $\overline{\nu}_{\rm max}$ is proportional to $r_T^{1/4}$.

A further general requirement determining $r_T^{\rm min}$ follows from the current limits (summarized in Table I) on the presence of relic graviton backgrounds in the audio band [23–26]. The parametrization of the spectral energy density adopted by Refs. [25,26] is in fact given by $\Omega_{gw}(\nu,\tau_0) = \overline{\Omega}_\sigma(\nu/\nu_{\rm ref})^\sigma$ so that, for instance, $\overline{\Omega}_0$ denotes the amplitude of the spectral energy density at $\nu_{\rm ref}$ for a scale-invariant slope. The three specific cases constrained in Refs. [25,26] are given in Table I however it is possible to find an interpolating formula valid for a handful of spectral indices (see e.g. [75]). By following here this approach we can broadly adopt the bounds of Table I and require

TABLE I. Recent limits on the relic gravitons obtained by wideband interferometers.

σ	Frequency range if $\nu_{\rm ref}$ [Hz]	Bound
0	20–81.9	$\overline{\Omega}_0 < 6 \times 10^{-8}$ Ref. [25]
2/3	20–95.2	$\overline{\Omega}_{2/3} < 4.8 \times 10^{-8}$ Ref. [25]
3	20–301	$\overline{\Omega}_3 < 7.9 \times 10^{-9}$ Ref. [25]
0	20–76.6	$\overline{\Omega}_0 < 5.8 \times 10^{-9}$ Ref. [26]
2/3	20–90.6	$\overline{\Omega}_{2/3} < 3.4 \times 10^{-9}$ Ref. [26]
3	20–291.6	$\overline{\Omega}_3 < 3.9 \times 10^{-10}$ Ref. [26]

$$10^{-12} \leq h_0^2 \Omega_{gw}(\nu_{\rm LVK}, \tau_0) < 10^{-10}, \qquad \nu_{\rm LVK} = \mathcal{O}(100)\ {\rm Hz}, \tag{4.4}$$

where $\nu_{\rm LVK}$ denotes the Ligo-Virgo-Kagra frequency which can be estimated in terms of $\nu_{\rm ref}$. The most sensitive region for the detection of relic gravitons in the audio band is, grossly speaking, below 0.1 kHz since, in this band, the overlap reduction function has its first zero [39]. Equation (4.4) requires, in practice, that the bounds coming from wideband interferometers are satisfied while, in the same frequency range, $h_0^2 \Omega_{gw}(\nu, \tau_0)$ is larger than 10^{-12}. We cannot foresee when the corresponding sensitivity will be reached by wideband detectors but the requirement of Eq. (4.4) follows from some of the optimistic claims suggested by the observational collaborations[19] [26]. By following a similar attitude, we shall enforce the big bang nucleosynthesis bound for all the ranges of the spectrum (and, in particular, at high frequencies) but also assume that that $h_0^2 \Omega_{gw}(\nu, \tau_0) > \mathcal{O}(10^{-8})$ for typical frequencies $\nu = \mathcal{O}(\nu_{\rm max})$. This means, on the one hand, that the bound of Eq. (3.7) is enforced while, at the same time, it is not excluded that the signal from the relic gravitons could be interesting for a direct detection with microwave cavities [75] in a range that encompasses the MHz and the GHz regions. In this regime coupled microwave cavities with superconducting walls [76–81], wave guides [82–86] or even small interferometers [87–89] could be used for direct detection even if the current sensitivities should not be overestimated without reason (see, in this respect, [75]).

A. Spike in the ultra-high-frequency region

The interplay between the high-frequency determinations of the spectral energy density and the low-frequency limits on r_T can be analytically deduced by considering the MHz and the GHz bands where the frequencies $\nu = \mathcal{O}(\nu_{\rm max})$ are approximately located. In this case the most constraining class of bounds follows by requiring that $\nu \to \nu_{\rm max}$ in Eq. (4.4) and by examining a (single) postinflationary phase parametrized by δ and ξ. Equation (3.7) should then be satisfied together with the condition that $h_0^2 \Omega_{gw}(\nu_{\rm max}, \tau_0) > 10^{-8}$; putting everything together we therefore obtain the approximate condition

$$10^{-8} \leq h_0^2 \Omega_{gw}(\nu_{\rm max}, \tau_0) < 5.61 \times 10^{-6} \Delta N_\nu n_T^{\rm high}. \tag{4.5}$$

In Eq. (4.5) the high-frequency spectral index appears if the parametrize the high-frequency behavior with a single slope $n_T^{\rm high}$; this is actually the most constraining instance even if the spikes may also arise at lower frequencies where, however, the corresponding amplitude is necessarily smaller since the frequency range for a potential growth of $h_0^2 \Omega_{gw}(\nu, \tau_0)$ is narrower. With these specifications we actually have from Eq. (3.7) that[20]

$$h_0^2 \int_{\nu_{bbn}}^{\nu_{\rm max}} \Omega_{gw}(\nu, \tau_0) d\ln\nu = \frac{h_0^2 \Omega_{gw}(\nu_{\rm max}, \tau_0)}{n_T^{\rm high}} \left[1 - \left(\frac{\nu_{bbn}}{\nu_r}\right)^{n_T^{\rm high}}\right] < 5.61 \times 10^{-6} \Delta N_\nu. \tag{4.6}$$

In Fig. 7 we illustrate the allowed region of the parameter space in the plane defined by δ and by $y = \log H_r/M_P$. Since $\xi = H_r/H_1$ implicitly contains a dependence upon r_T, the various constraints are illustrated in the (y, δ) plane where y denotes the common logarithm of (H_r/M_P). In the left plot of Fig. 7 all the different constraints are superimposed while the overlapping region is directly illustrated in the plot at the right.

The shaded area in the right plot of Fig. 7 corresponds then to $r_T = 3 \times 10^{-2}$ which is of the order of one of the most stringent constraints on r_T available at the moment[21] [8–10]. The logic is now to decrease progressively the value of r_T and, in doing so, the area of the overlap of Fig. 7 is expected to shrink. If the allowed region originally present in Fig. 7 completely disappears, the value of r_T will be by definition smaller than $r_T^{\rm min}$. The gradual decrease is illustrated in Fig. 8 where the values of r_T are reduced first to 3×10^{-4} (plot at the left) and then to 3×10^{-5} (upper part of the right plot). The lower region of the right plot corresponds to $r_T = 3 \times 10^{-6}$. If the value of r_T is

[19]The alternative would be that relic gravitons backgrounds will not be accessible in the audio band; while this possibility cannot be excluded, in what follows we shall entertain a less pessimistic attitude which is motivated by the steady increase of the sensitivity to relic gravitons in the last 20 years. We must actually recall that in 2004 wideband detectors gave limits implying $h_0^2 \Omega_{gw}(\nu, \tau_0) < \mathcal{O}(1)$ [23] while today the same limits improved by roughly 10 orders of magnitude [25,26].

[20]The upper limit of Eq. (4.5) follows from Eq. (4.6) in the case $n_T^{\rm high} > 0$ and $\nu_r > \nu_{bbn}$ [which is the same condition already discussed in Eq. (4.2)].

[21]In Fig. 7 we also fixed $g_{s,eq} = g_{\rho,eq} = 3.94$ and $g_{s,r} = g_{\rho,r} = 106.75$ implying that $\mathcal{C}(g_s, g_\rho) = 0.75$. Different values of the late-time parameters have a comparatively small effect on the shape of the allowed region.

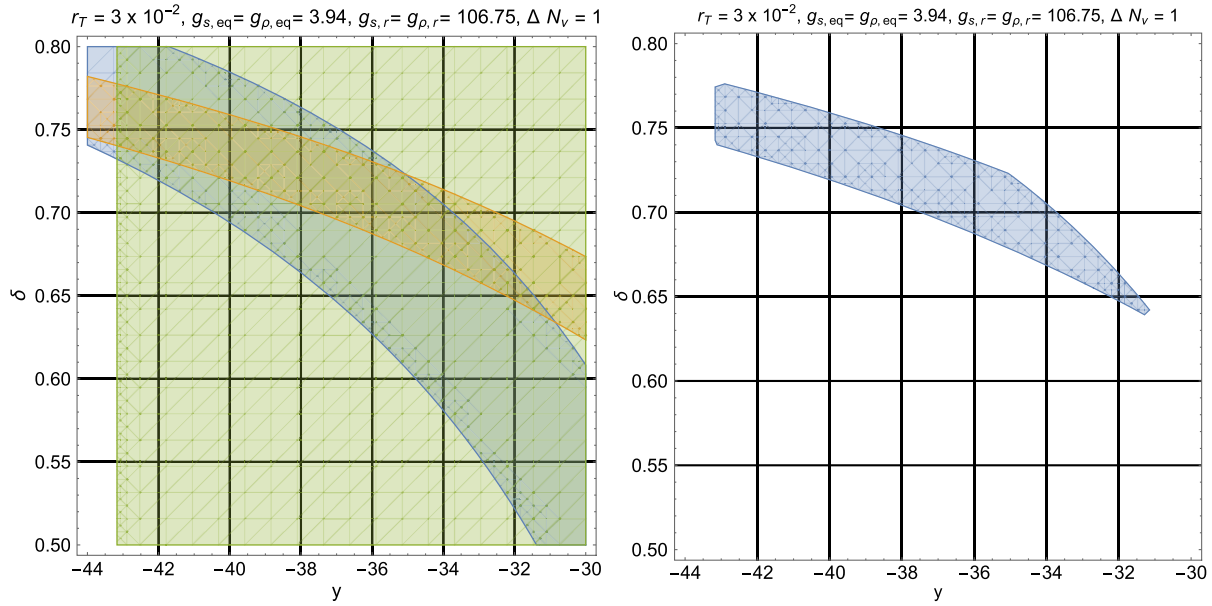

FIG. 7. Since ξ contains a dependence on r_T, it is preferable to plot (on the horizontal axis) the common logarithm of H_r/M_P [i.e. $y = \log(H_r/M_P)$] which does not contain r_T. We assumed here that $r_T \to 0.03$; in the plot at the *left* all the different limits [see Eqs. (4.2), (4.4) and (4.5)] have been superimposed in the plane (y, δ). In the plot at the right the intersection of the three regions [defined, respectively, by Eqs. (4.2), (4.4) and (4.5)] is directly illustrated. The values of the late-time parameters considered in this and in the following figure lead approximately to $\mathcal{C}(g_s, g_\rho) = 0.75$; these terms are included even if they are not essential for the quantitative assessment of the various bounds.

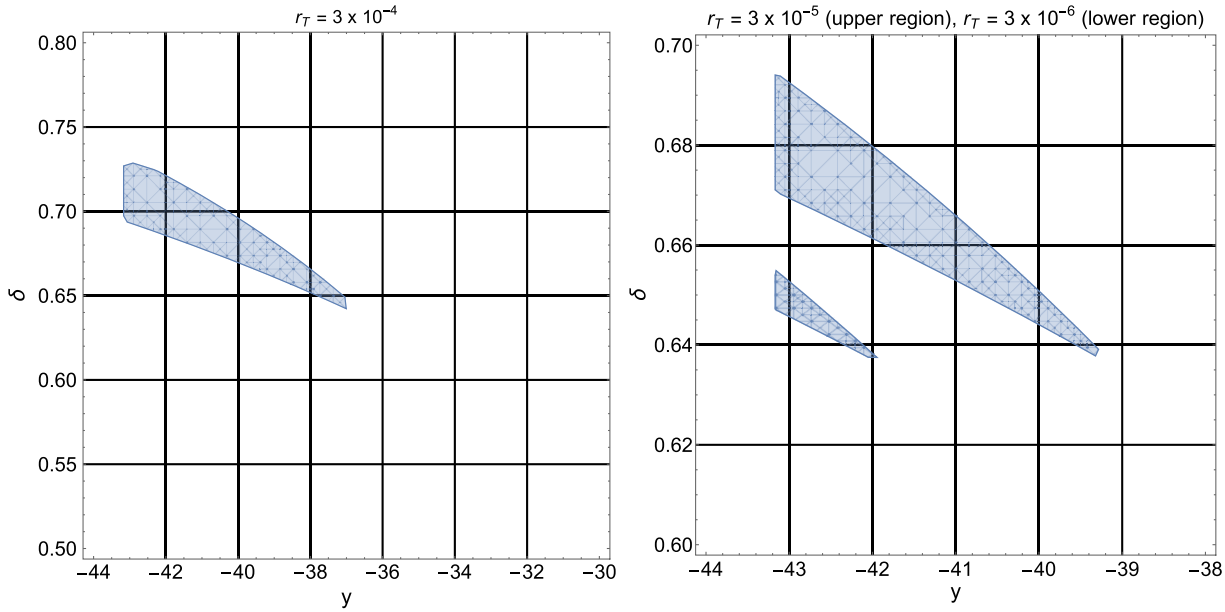

FIG. 8. The value of r_T is gradually reduced while all the remaining late-time parameters are kept fixed. In the left plot the shaded region corresponds to $r_T = 3 \times 10^{-4}$. In the right plot there are two different regions: in the upper spot $r_T = 3 \times 10^{-5}$ while in the lower spot $r_T = 3 \times 10^{-6}$. If the value of r_T is further reduced to 3×10^{-7}, then the intersection of the different constraints illustrated in Fig. 7 completely disappears and this occurrence implies that $r_T^{\mathrm{min}} = \mathcal{O}(10^{-6})$. To characterize better the different regions the two plots have different ranges of δ: this is while the upper region of the right plot seems superficially larger than the area of the left plot.

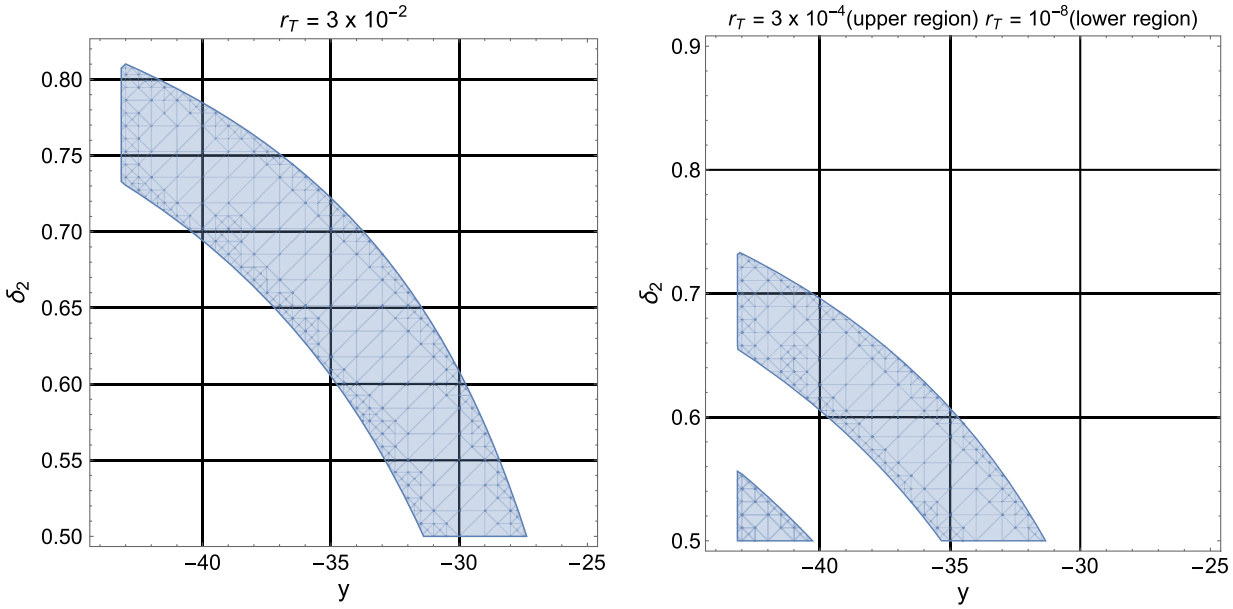

FIG. 9. We analyze the case of spike in the audio band. In the two plots the shaded regions correspond, respectively, to $r_T = 3 \times 10^{-2}$ (plot at the left) and to $r_T = 3 \times 10^{-4}$ (plot at the right). The lower region in the plot at the right is obtained for $r_T = 10^{-8}$.

further reduced to $r_T = 3 \times 10^{-7}$, then the lower spot completely disappears from the figure. We therefore conclude that the tensor-to-scalar ratio should exceed $r_T^{\rm min} = \mathcal{O}(10^{-6})$ if the spectral energy density of the relic gravitons exhibit a potential signal in high-frequency band.

B. Spike in the audio band

The analysis of the high-frequency region can be repeated at lower frequencies and, in particular, in the audio band. By looking at Eqs. (3.17) and (3.18) the most constraining situation is the one where the frequency of the signal falls exactly in the audio band [i.e. $\nu_2 = \mathcal{O}(\nu_{\rm audio})$]. If, prior to radiation dominance, the expansion rate is first faster than radiation and then slows down, then the spectral energy density exhibits a local maximum in ν_2 and this is the situation already illustrated in Fig. 6. The high-frequency slopes of $h_0^2\Omega_{gw}(\nu, \tau_0)$ are positive for $\nu < \nu_2$ (i.e. $n_2^{\rm high} > 0$) and negative in the complementary frequency range (i.e. $n_1^{\rm high} < 0$ for $\nu > \nu_2$). If the timeline of the comoving horizon is inverted (and the background expands first slower than radiation and then faster) in ν_2 there will be a minimum with a spectral energy density even smaller than in the case of the concordance scenario where $h_0^2\Omega_{gw}(\nu, \tau_0) = \mathcal{O}(10^{-17})$. The constraints at higher frequencies can be neglected since the signal is automatically small for $\nu = \mathcal{O}(\nu_{\rm max})$ and the bounds stemming from the expansion rate at the nucleosynthesis time are automatically satisfied. The results of the analysis are summarized in Fig. 9 where the late-time parameters have been selected as in Figs. 7 and 8. In the left plot of Fig. 9 we have chosen $r_T = 3 \times 10^{-2}$ while in the right plot the two shaded spots correspond, respectively, to $r_T = 3 \times 10^{-4}$ (upper region) and to $r_T = 10^{-8}$ (lower region). If r_T is further reduced below 10^{-8} the different requirements are not concurrently satisfied and we must therefore conclude that, in this case, $r_T^{\rm min} = \mathcal{O}(10^{-7})$.

There is the possibility, in principle, that the spike of the spectral energy density might occur in nHz region. In this instance the current measurements of the PTA could be relevant to set a limit on r_T. The PTA reported in fact a tentative signal in the nHz band:

$$10^{-8.86} b_0^2 < h_0^2\Omega_{gw}(\nu) < b_0^2 10^{-9.88}, \qquad 3\ {\rm nHz} < \nu < 100\ {\rm nHz}, \tag{4.7}$$

where b_0 depends on the different experiments. The Parkes Pulsar Timing Array collaboration [28] suggests $b_0 = 2.2$; the International Pulsar Timing Array gives $b_0 = 2.8$ [30] while the European Pulsar Timing Array [29] would measure $b_0 = 2.95$. These results are compatible with the NANOgrav 12.5 yrs data [27] implying $b_0 = 1.92$. From the average of the four measurements presented so far we obtain $\overline{b}_0 = 2.467$ which implies[22]

$$10^{-9.09}\left(\frac{\overline{b}_0}{2.467}\right)^2 \leq h_0^2\Omega_{gw}(\nu) \leq 10^{-8.07}\left(\frac{\overline{b}_0}{2.467}\right)^2. \tag{4.8}$$

[22]If $b_0 \to 1$, then Eq. (4.7) would suggest that the energy density in the nHz domain is comparatively smaller than the Ligo-Virgo-Kagra constraint for a flat spectrum [26]; however, according to current determinations, $b_0 > 1$.

The constraints of Eqs. (4.7) and (4.8) are only marginally relevant in the present case. Indeed, recalling Eq. (4.2) we have that, at most, $\nu_r = \mathcal{O}(10^{-2})$ nHz. To be relevant for Eq. (4.7) the spectral energy density should be sufficiently large for $\nu = \mathcal{O}(100)$ nHz. Taking into account that, at most, $h_0^2\Omega_{gw}(\nu_r, \tau_0) \leq \mathcal{O}(10^{-17})$ it follows that a spike for $\nu_{\rm spike} = \mathcal{O}(100)$ nHz can only be $h_0^2\Omega_{gw}(\nu_{\rm spike}, \tau_0) \leq \mathcal{O}(10^{-13})$ since, at most, the slope of the spectral energy density between ν_r and $\nu_{\rm spike}$ can be linear.[23] Before concluding this discussion it is appropriate to stress that the values of the various δ_i have been always assumed to be larger than $1/2$. The reason for this choice is that this is what happens in all the relevant physical situations. In the case of a stiff fluid we have that $1/2 \leq \delta < 1$; smaller values of δ correspond to sound speeds of the plasma larger than the speed of light. In the case of the scalar potentials discussed in Eq. (2.30) $\delta \to 1/2$ for $q \gg 1$.

C. Constraints, specific potentials and compensations

The results obtained so far assume the enforcement of the consistency relations and, in the opposite case, it is always possible to reduce the spectral energy density in the aHz region by keeping a comparatively larger signal in the higher frequency range. The bounds obtained here suggest

$$r_T > r_T^{\rm min} = \mathcal{O}(10^{-7}), \qquad \nu = \mathcal{O}(\nu_{\rm audio}),$$
$$r_T > r_T^{\rm min} = \mathcal{O}(10^{-6}), \qquad \nu = \mathcal{O}(\nu_{\rm max}). \tag{4.9}$$

The reference to the frequency range simply reminds that, in the two cases, the most constraining situation correspond to the presence of a spike around either $\nu_{\rm audio}$ or $\nu_{\rm max}$. The results of Eq. (4.9) are now illustrated by few examples based on the different classes of potentials discussed in Sec. II and in Appendix B. In this respect the first point to bear in mind is that the number of e-folds depends both on r_T and on the post-inflationary evolution but the relative impact of the two contributions is different. We recall that N_k actually measures the number of e-folds since the crossing of the CMB scale and if the postinflationary evolution is slower than radiation N_k is larger than 60; similarly if r_T is smaller also N_k diminishes. Let us examine, for the sake of concreteness, the expression of N_k given in Eq. (A10), which we rewrite by enforcing the consistency relations[24]

$$N_k = \mathcal{O}(60) + \frac{1}{4}\ln\left(\frac{r_T}{0.03}\right) + \frac{1}{2}\sum_{i=1}^{n-1}\left(\frac{\delta_i - 1}{\delta_i + 1}\right)\ln\xi_i. \tag{4.10}$$

For the reasons explained in Eqs. (B4) and (B6) we used that $H_k/H_1 = \mathcal{O}(1)$ since this way of writing N_k is more suitable. As already stressed in different frameworks [20,21,90] the existence of postinflationary phases with sound speed stiffer than radiation entails an *increase* both of N_k and of $N_{\rm max}$ [see Eqs. (A7) and (A8) and discussion therein]. Within the notations of Eq. (4.10) we have indeed that when some of the $\delta_i < 1$ (and the background expands slower than radiation) $N_k \gg 60$ depending on the various ξ_i which are always, by definition, smaller (or even much smaller) than 1. In the past various upper bounds on the potential increase of N_k have been set; within these attempts we can conceivably assume that N_k and $N_{\rm max}$ may increase by a factor[25] $\mathcal{O}(15)$. When N_k is larger than in the standard case the tensor to scalar ratio and the scalar spectral index may be comparatively more suppressed and their values must then be confronted again with Eqs. (2.33)–(2.35).

Indeed as we specifically discussed in the previous examples [see e.g. (2.39) and (2.40)] the scale dependence of r_T and n_s is mediated by N_k, i.e. $r_T(k) = r_T(N_k)$ and $n_s(k) = n_s(N_k)$. It becomes therefore a quantitative issue if the amount of reduction of $r_T(N_k)$ for $N_k \gg \mathcal{O}(60)$ is compatible with $n_s(N_k)$ and with the (upper) bounds on r_T of Eqs. (2.33)–(2.35). Based on the bounds of Eq. (4.9) and on the results of the previous sections we then expect $r_T(N_k) > r_T^{\rm min} = \mathcal{O}(10^{-7})$ [or even $\mathcal{O}(10^{-6})$] provided the signal of high-frequency gravitons is still sufficiently large. In this respect the first test is reported in Figs. 10 and 11 where we examine the plateaulike potential of Eq. (2.37) in the plane defined by $y = \log H_r/M_P$ and by q. While for $\Phi \gg 1$ the inflationary phase fixes $n_s(N_k)$ and $r_T(N_k)$ according to Eqs. (2.39) and (2.40), for $\Phi < 1$ there is an oscillating stage whose length is here taken as a free parameter. During this stage the expansion rate δ follows from Eqs. (2.28) and (2.29). In Figs. 10 and 11 the shaded areas correspond to the region where the scalar spectral index and the r_T obey the constraints of Eq. (2.35) and all the other high-frequency limits. We also require that $10^{-8} < h_0^2\Omega_{gw}(\nu, \tau_0) < 10^{-6}$ for $\nu = \mathcal{O}(\nu_{\rm max})$ (with the caveat that also $\nu_{\rm max}$ depends on δ).

In the left plot of Fig. 10 we fixed p while in the right plot q is fixed. The same strategy has been adopted in Fig. 11 for a different set of parameters. The various curves appearing in Figs. 10 and 11 correspond to the common logarithms of $r_T(N_k)$. We see, as expected, that these values are all larger than $r_T^{\rm min}$. It is relevant to stress that Figs. 10

[23]This means that a spike on the nHz band is always smaller than the figures suggested by Eqs. (4.7) and (4.8). The nature of the PTA observations is still under debate and it cannot be excluded that the potential signal is not related with the relic gravitons.

[24]If we compute N_k from Eq. (A10) and use the consistency relations together with the explicit value of $\mathcal{C}(g_s, g_\rho)$, then we would obtain 59.58 and this is why we wrote $\mathcal{O}(60)$ in Eq. (4.10); as we shall see these differences are immaterial for this discussion.

[25]This estimate follows from Eq. (4.10) by considering the smallest value of δ compatible with standard sources (i.e. $\delta \to 1/2$) and by taking the minimal value of ξ compatible with the ΛCDM paradigm; we get in this case $\Delta N_k = (1/6)\ln\xi_{\rm min} = \mathcal{O}(15)$ for $\xi_{\rm min} = \mathcal{O}(10^{-38})$.

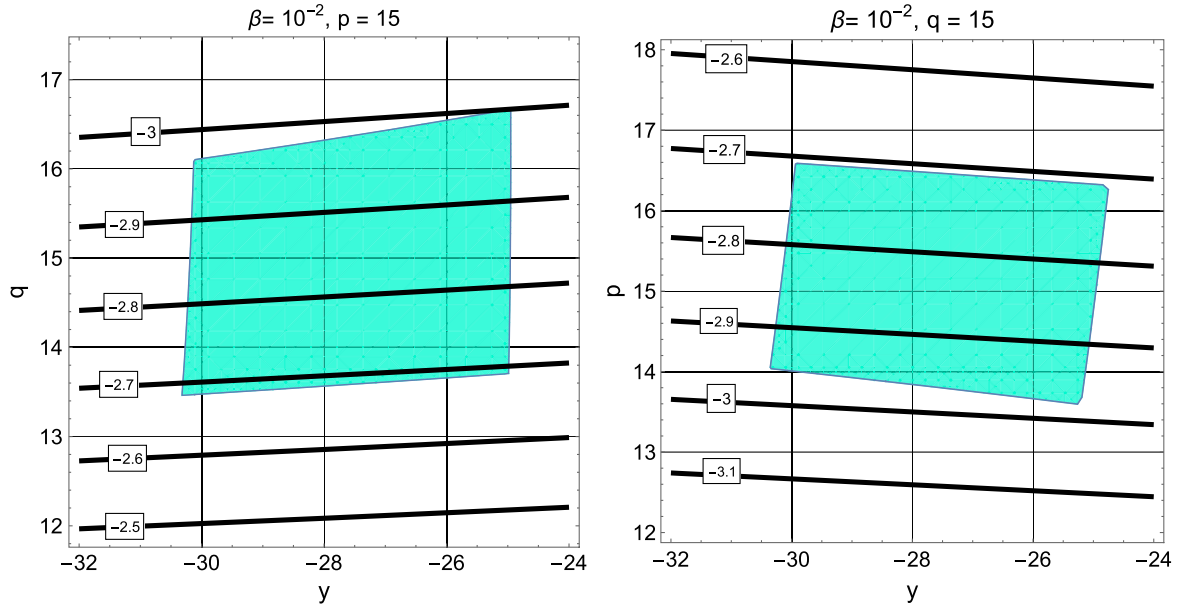

FIG. 10. We evaluate the allowed values of $n_s(N_k)$ and $r_T(N_k)$. As in the previous plots y denotes the common logarithm of H_r/M_P (i.e. $y = \log H_r/M_P$). In the plot at the left the value of p is fixed while in the plot at the right q is fixed. In the shaded regions $n_s(N_k)$ and $r_T(N_k)$ fall within the constraints of Eq. (2.35) and simultaneously lead to a large signal for frequencies $\mathcal{O}(\nu_{\rm max})$. In both plots we can verify that $r_T(N_k) > r_T^{\rm min}$ implying the validity of the general bound deduced in Eq. (4.9).

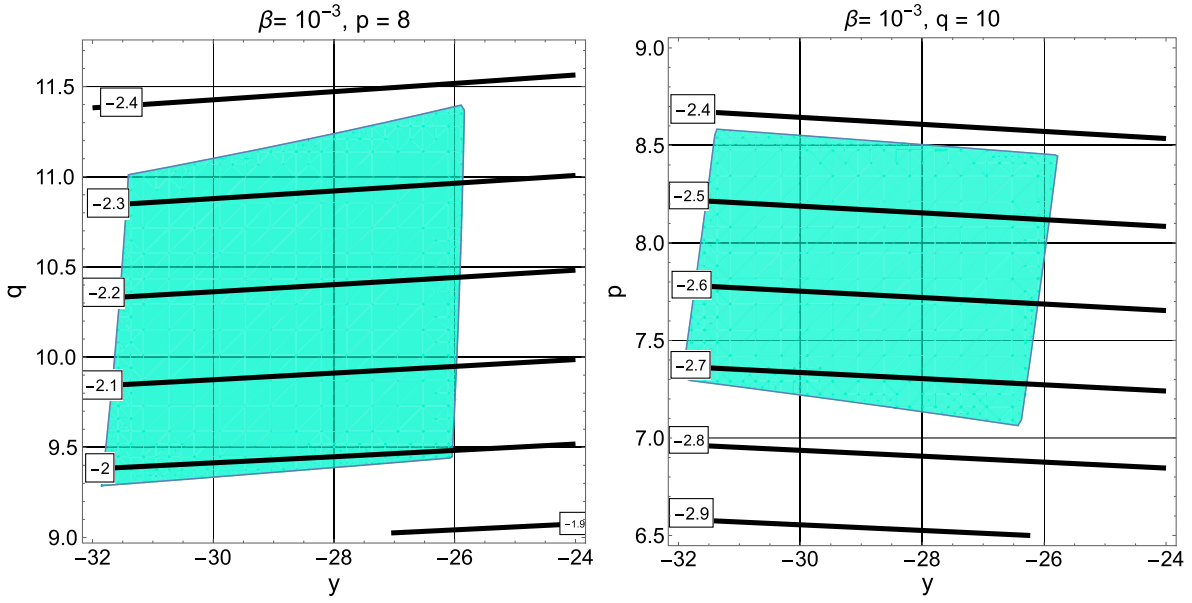

FIG. 11. The same notations of Fig. 10 have been followed for a different choice of the parameters. In both cases $r_T(N_k) > r_T^{\rm min}$. We see that, also in this case, the values of r_T in the allowed region are larger than $r_T^{\rm min}$.

and 11 have been obtained by assuming the dynamical determination of N_k as suggested by Eq. (4.10). On the contrary in the case of Figs. 3 and 4 $N_k = 60$ as if the postinflationary evolution was absent. Both illustrative strategies have their own virtues but we think that the former is more consistent than the latter especially in the case where a long oscillating stage with $q > 2$ implies an expansion rate that is slower than radiation.

So far we explored the regime of relatively large r_T and we now consider the opposite limit by requiring that the high-frequency signal is (systematically) small while all the other low-frequency constraints are satisfied. As already

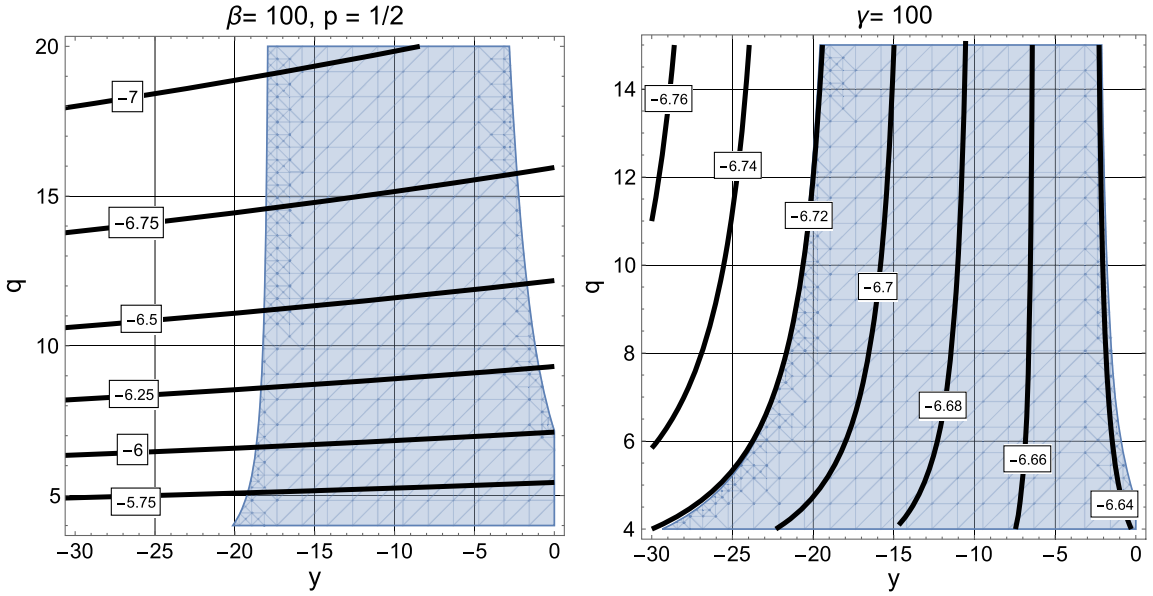

FIG. 12. We illustrate the situation where the high-frequency signal is small while the low-frequency bounds of Eq. (2.35) are concurrently satisfied. In the plot at the left we always consider the potential of Eq. (2.37) while at the right the potential is given by Eq. (2.38). In both plots the shaded area corresponds to $10^{-25} < h_0^2\Omega_{gw}(\nu_{\rm max}, \tau_0) < 10^{-15}$ and the various labels denote the common logarithm of r_T. We see, as expected, that $r_T < \mathcal{O}(r_T^{\rm min})$.

mentioned in Sec. II a potential candidate for rather small r_T is represented by the hilltop models in their different versions [48–52]. Here we are considering a slightly different perspective by focussing on the potentials of Eqs. (2.37) and (2.38) where, however, N_k includes the dependence of a postinflationary stage expanding slower than radiation as suggested by Eq. (4.10).

This analysis is illustrated in Fig. 12 where the low-frequency constraints of Eq. (2.35) are supplemented by the requirement $10^{-25} < h_0^2\Omega_{gw}(\nu_{\rm max}, \tau_0) < 10^{-15}$. According to the general arguments given above we should have that $r_T(N_k) = \mathcal{O}(10^{-6})$ (or smaller). According to Fig. 12 this is what happens. More precisely in the left plot of Fig. 12 we consider the potential of Eq. (2.37) but for a range of parameters different from the ones discussed before. The shaded area now defines the region of the parameter space where the spectral energy density is smaller than 10^{-15} (but larger than 10^{-25}). This is approximately the standard signal of the concordance paradigm. In the plot at the right the notations are the same but the potential is the one of Eq. (2.38).

There is finally an extreme situation where a drastic decrease of r_T is compensated by the contribution of the postinflationary stage of expansion. Indeed, by looking at Eq. (4.10) we might argue that the decrease in the number of e-folds caused by a reduction of r_T could compensated by a corresponding increase of the term $\mathcal{D}(\delta_i, \xi_i)$ so that, overall, $N_k = \mathcal{O}(60)$. This cancellation implies that the postinflationary stage must expand slower than radiation and, in this case,

$$r_T \simeq \mathcal{D}^2(\delta_i, \xi_i) = \prod_{i=1}^{n-1} \xi^{-2(\delta_i - 1)/(\delta_i + 1)} \ll \mathcal{O}(0.03). \tag{4.11}$$

For a single postinflationary stage we would have that $r_T \simeq \xi^{-2(\delta-1)/(\delta+1)}$ with $0 < \delta < 1$. From Eqs. (3.8) and (3.11) we therefore have that the high-frequency value of the spectral energy density is approximately given by $h_0^2\Omega_{gw}(\nu_{\rm max}, \tau_0) = \mathcal{O}(10^{-18})$, slightly smaller than in the case of the concordance scenario. This means that a very small r_T [e.g. much smaller than $\mathcal{O}(10^{-6})$] can be compensated by a long postinflationary stage expanding slower than radiation. In this case, however, the spectral energy density is just shifted below the signal of the concordance paradigm.

V. CONCLUDING REMARKS

The limits on the relic graviton backgrounds in different domains of comoving frequencies have been combined with the purpose of narrowing the range of variation of the tensor-to-scalar ratio. In the concordance paradigm the low-frequency tail of the aHz region is maximized by considering the largest r_T compatible with the available observational data. In this investigation we explored the opposite possibility suggesting that the low-frequency gravitons could remain practically invisible in the aHz region while their spectral energy density exceeds the predictions of the concordance paradigm at higher frequencies. As a result, depending on the frequency domain of the

spike the lower bound on the tensor-to-scalar ratio ranges between $\mathcal{O}(10^{-6})$ and $\mathcal{O}(10^{-7})$.

The obtained results do not depend on the shape of the inflationary potential since the relic gravitons couple predominantly to the space-time curvature and not to the matter sources. We nonetheless enforced the consistency relations and corroborated the obtained bound with the detailed discussion of various classes of inflationary potentials admitting a modified postinflationary evolution and eventually leading to a high-frequency spike. In the present framework the number of e-folds corresponding to the exit of the CMB wavelengths can be larger than $\mathcal{O}(60)$ if the postinflationary expansion rate is slower than radiation. If the consistency relations are instead violated (for instance because of the properties on the initial state or for some other reason), then r_T can be further reduced without affecting the high-frequency signal and the lower bounds derived here do not apply. The general logic remains however intact since the reduction of the tensor-to-scalar ratio would not preclude spectral energy densities exceeding the ones of the concordance scenario at high frequencies.

Since the concurrent determinations stemming from the audio band and from the aHz region involve the postinflationary evolution, in the present approach any potential upper limit at high frequency simultaneously constrain the expansion rate prior to radiation dominance and the tensor-to-scalar ratio. This perspective implicitly encourages a synergy between experiments scrutinizing different branches of the graviton spectrum. The fruitful dialog between the instruments sensitive to small and to intermediate frequencies could be extended, in principle, also to conceptually different kinds of detectors in the MHz domain as repeatedly suggested in the past.

ACKNOWLEDGMENTS

I wish to thank T. Basaglia, A. Gentil-Beccot, S. Reyes, S. Rohr and J. Vigen of the CERN Scientific Information Service for their valuable help. Various discussions with the late E. Picasso on high-frequency gravitons are also acknowledged.

APPENDIX A: THE NUMBER OF e-FOLDS AND THE MAXIMAL FREQUENCY

1. Number of e-folds and crossing of the pivot scales

In what follows and in the bulk of the paper[26] $N_k = \ln(a_1/a_k)$ denotes the number of e-folds corresponding to the crossing of a given wavelength and a_1 conventionally sets the end of the inflationary stage of expansion. Since the inflationary epoch may be followed by a sequence of different phases all characterized by their own expansion rates δ_i [i.e. $a_i(\tau) \propto \tau^{\delta_i}$ in the conformal time parametrization] the values of N_k are implicitly determined from

$$\frac{k}{a_k H_k} = e^{N_k}\left(\frac{H_1}{H_k}\right)\frac{k}{a_1 H_1}, \tag{A1}$$

and the general evolution of the comoving horizon is illustrated in Fig. 1. When the given wavelength crosses the Hubble radius in Fig. 1 (i.e. $k \simeq a_k H_k$) Eq. (A1) fixes the value of N_k not only in terms of H_1 (the expansion rate at the end of inflation) but also as a function of the subsequent expansion history. We can appreciate this statement by expressing the last term at the right-hand side of Eq. (A1) as

$$\frac{k}{a_1 H_1} = \frac{k}{a_0 H_0}\left(\frac{a_0 H_0}{a_{eq} H_{eq}}\right)\left(\frac{a_{eq} H_{eq}}{a_r H_r}\right)\left(\frac{a_r H_r}{a_1 H_1}\right), \tag{A2}$$

where H_r is the expansion rate at the moment of radiation dominance while H_{eq} and H_0 denote, respectively, the expansion rates at equality and at the present time; we remind that, in the notations of Fig. 1, $H_n = H_r$ and $a_n = a_r$, as already discussed in the bulk of the paper. From Eqs. (A1) and (A2) we can also deduce

$$\frac{k}{a_k H_k} = \left(\frac{k}{a_0 H_0}\right)\frac{\sqrt{H_0/M_P}}{(2\pi\Omega_{R0}\epsilon_k \mathcal{A}_{\mathcal{R}})^{1/4}}\frac{\sqrt{H_1/H_k}}{\mathcal{C}(g_s, g_\rho)}\mathcal{D}(\delta_i, \xi_i)e^{N_k}. \tag{A3}$$

In Eq. (A3) $\mathcal{C}(g_s, g_\rho)$ and $\mathcal{D}(\delta_i, \xi_i)$ depend, respectively, on the radiative evolution after a_r and on the postinflationary history between the end of inflation and the moment of radiation dominance:

$$\mathcal{C}(g_s, g_\rho) = (g_{s,eq}/g_{s,r})^{1/3}(g_{\rho,r}/g_{\rho,eq})^{1/4},$$
$$\mathcal{D}(\delta_i, \xi_i) = \prod_{i=1}^{n-1}\xi_i^{-\frac{(\delta_i - 1)}{2(\delta_i + 1)}}. \tag{A4}$$

The first expression of Eq. (A4) follows by considering the radiation-dominated evolution between a_r and a_{eq}; in this case we exactly obtain that $(H_r/H_{eq})^{1/2} = (a_{eq}/a_r)\mathcal{C}(g_s, g_\rho)$ since in a stage of local thermal equilibrium, the entropy density is conserved and the total energy density depends on g_ρ (i.e. the number of relativistic degrees of freedom in the plasma) while g_s denotes the effective number of relativistic degrees of freedom appearing in the entropy density. In the standard situation where $g_{s,r} = g_{\rho,r} = 106.75$ and $g_{s,eq} = g_{\rho,eq} = 3.94$ we have that $\mathcal{C}(g_s, g_\rho) = 0.75$. The contribution of $\mathcal{C}(g_s, g_\rho)$ to Eq. (A3) is numerically not essential for the determination of N_k and the term $\mathcal{D}(\delta_i, \xi_i)$ has a more prominent effect. Indeed, as already mentioned, in Eq. (A4) δ_i estimates the expansion rate in each of the postinflationary

[26] As already mentioned in the introduction $\ln x$ denotes the natural logarithm of a generic variable x; $\log x$ denotes instead the common logarithm of the same quantity.

stages and $\xi_i = H_{i+1}/H_i < 1$ measures their relative duration. In the limit of a single postinflationary phase all the δ_i collapse to a single δ and $\mathcal{D}(\delta,\xi) = \xi^{-(\delta-1)/[2(\delta+1)]}$, where $\xi = H_r/H_1 < 1$.

The constraints from big bang nucleosynthesis suggest an absolute lower limit on ξ (i.e. $H_r \geq 10^{-44} M_P$) since the plasma must be dominated by radiation as soon as the formation of light nuclei starts and, for the same reason, the product of all the ξ_i equals H_r/H_1, i.e. by definition $\xi_1\xi_2\ldots\xi_{n-1}\xi_n = \xi = H_r/H_1$. The actual value of $\xi = H_r/H_1$ ultimately depends on H_1 whose explicit estimate follows by remarking that[27]

$$\left(\frac{H_k}{M_P}\right) = \sqrt{\pi\epsilon_k \mathcal{A}_{\mathcal{R}}}, \qquad \left(\frac{H_k}{H_1}\right) = \mathcal{O}(1). \tag{A5}$$

Besides the number of e-folds associated with the crossing of a given scale k there is also a second relevant notion, namely the *maximal number of e-folds presently accessible to large-scale observations* ($N_{\rm max}$ in what follows). This quantity is determined by fitting the (redshifted) inflationary event horizon inside the current Hubble patch, i.e. $H_b^{-1}(a_0/a_i) \simeq H_0^{-1}$ where H_b denotes the expansion rate in the initial stages of inflation:

$$e^{N_{\rm max}} = (2\Omega_{R0})^{1/4}\sqrt{\frac{H_b}{H_0}}\frac{\mathcal{C}(g_s,g_\rho)}{\mathcal{D}(\delta_i,\xi_i)}, \qquad H_b = \mathcal{O}(H_1). \tag{A6}$$

In Eq. (A6) H_b can be estimated from H_1 owing from the small variation of the Hubble rate during inflation and the same observation can be actually made in the case of H_k, as we shall discuss in Appendix B. As in the case of N_k, in Eq. (A6) we assumed that the postinflationary expansion rate is partitioned in n subsequent epochs expanding at different rates but the last stage always coincides with radiation so that, by definition, $H_n = H_r$. The values of N_k and $N_{\rm max}$ are related as

$$N_k = N_{\rm max} - \ln\left(\frac{k}{a_0 H_0}\right) - \ln\frac{H_k}{H_1}. \tag{A7}$$

As we shall see more specifically in Appendix B $H_k = \mathcal{O}(H_1)$ for all the comoving wavelengths relevant in the case of CMB physics so that, in practice, $N_{\rm max}$ coincides with N_k when $k = \mathcal{O}(a_0 H_0)$. The explicit values of N_k and $N_{\rm max}$ enter the estimates the inflationary observables for a specific choice of the potential; for instance the value of $N_{\rm max}$ is

$$\begin{aligned} N_{\rm max} = {} & 61.55 - \ln\left(\frac{h_0}{0.7}\right) + \frac{1}{4}\ln\left(\frac{\epsilon}{0.001}\right) + \frac{1}{4}\ln\left(\frac{\mathcal{A}_{\mathcal{R}}}{2.41\times 10^{-9}}\right) + \ln\mathcal{C}(g_s,g_\rho) \\ & + \frac{1}{4}\ln\left(\frac{h_0^2\Omega_{R0}}{4.15\times 10^{-5}}\right) + \frac{1}{2}\sum_i^{n-1}\left(\frac{\delta_i - 1}{\delta_i + 1}\right)\ln\xi_i. \end{aligned} \tag{A8}$$

Equation (A8) depends on the slow-roll parameter ϵ which we have taken to be constant and scale independent. However if the consistency relations are enforced we can trade[28] ϵ for r_T since $r_T \simeq 16\epsilon$. Since the values of N_k and $N_{\rm max}$ are related we have from Eqs. (A2)–(A6) that

$$e^{N_k} = (2\Omega_{R0})^{1/4}\sqrt{\frac{H_k}{H_1}}\sqrt{\frac{H_k}{H_0}}\frac{\mathcal{C}(g_s,g_\rho)}{\mathcal{D}(\delta_i,\xi_i)}\left(\frac{k}{a_0 H_0}\right)^{-1}. \tag{A9}$$

We now recall (see also Appendix B) that $H_k/M_P = \sqrt{\pi\epsilon_k\mathcal{A}_{\mathcal{R}}}$; Eq. (A9) can then be written, after taking the natural logarithm of both sides,

$$\begin{aligned} N_k = {} & 59.4 + \frac{1}{4}\ln\left(\frac{\epsilon_k}{0.001}\right) + \frac{1}{4}\ln\left(\frac{\mathcal{A}_{\mathcal{R}}}{2.41\times 10^{-9}}\right) + \ln\mathcal{C}(g_s,g_\rho) - \ln\left(\frac{k}{0.002\ {\rm Mpc}^{-1}}\right) \\ & + \frac{1}{4}\ln\left(\frac{h_0^2\Omega_{R0}}{4.15\times 10^{-5}}\right) + \frac{1}{2}\sum_{i=1}^{n-1}\left(\frac{\delta_i - 1}{\delta_i + 1}\right)\ln\xi_i - \frac{1}{2}\ln\left(\frac{H_1}{H_k}\right). \end{aligned} \tag{A10}$$

[27]The result of Eq. (A5) has been implicitly used in Eq. (A3) and it is further analyzed in the subsequent Appendix B.

[28]In this case, if $r_T = \mathcal{O}(0.06)$ we would have that $N_{\rm max} = 61.88$ always assuming the typical values of the other parameters; if the explicit value of $\mathcal{C}(g_s,g_\rho)$ is taken into account the value of $N_{\rm max}$ is insignificantly reduced to $N_{\rm max} = 61.61$.

If we set $\delta_i = 1$ into Eqs. (A8)–(A10), then we obtain the standard result implying that $N_{\rm max} = \mathcal{O}(60)$; in this case the whole postinflationary stage collapses to a single radiation-dominated phase extending down to the H_r. If $\delta_i < 1$, then we have instead $N_{\rm max} > 60$ and this happens since all the ξ_i are, by definition, all smaller than 1; for the same reason $N_{\rm max} < 60$ when $\delta_i > 1$. For a single phase expanding slower than radiation $N_{\rm max}$ can be as large as 75 and in all the intermediate situations (where there are different phases expanding either faster or slower than radiation) $N_{\rm max}$ depends on the relative duration of the various epochs and on their expansion rates. What is true for $N_{\rm max}$ is also true for N_k by virtue of Eq. (A7). In the case of a specific potential admitting a postinflationary stage not dominated by radiation the correct value of N_k employed to evaluate the inflationary observables must then follow from Eq. (A10).

2. The typical frequencies of the spectrum

As in the case of N_k and $N_{\rm max}$, all the typical frequencies depend on r_T and on the postinflationary expansion rate (see also the cartoon of Fig. 1). Starting from $\nu_{\rm max}$ we have

$$\nu_{\rm max} = \prod_{i=1}^{n-1} \xi_i^{\frac{\delta_i - 1}{2(\delta_i+1)}} \overline{\nu}_{\rm max} = \mathcal{D}^{-1}(\delta_i, \xi_i)\overline{\nu}_{\rm max}. \tag{A11}$$

Note that when all the $\delta_i \to 1$ the value of $\nu_{\rm max}$ coincides with $\overline{\nu}_{\rm max}$ whose explicit value is

$$\overline{\nu}_{\rm max} = \frac{M_P}{2\pi}(2\Omega_{R0})^{1/4}\sqrt{\frac{H_0}{M_P}}\sqrt{\frac{H_1}{M_P}}\mathcal{C}(g_s, g_\rho). \tag{A12}$$

Both $\nu_{\rm max}$ and $\overline{\nu}_{\rm max}$ are computed from the smallest wavelength that crosses the Hubble radius of 1 and immediately reenters; this is why Eq. (A12) depends upon H_1. From a quantum mechanical viewpoint the maximal frequency corresponds to the production of a single graviton pair. In view of a direct estimate of $\overline{\nu}_{\rm max}$ we recall again that $H_1 = \mathcal{O}(H_k)$ [see Eq. (A5) and discussion therein]:

$$\overline{\nu}_{\rm max} = 195.38\mathcal{C}(g_s, g_\rho)\left(\frac{\mathcal{A}_\mathcal{R}}{2.41\times 10^{-9}}\right)^{1/4}\left(\frac{\epsilon_k}{0.001}\right)^{1/4} \times \left(\frac{h_0^2\Omega_{R0}}{4.15\times 10^{-5}}\right)^{1/4} \text{MHz}. \tag{A13}$$

In case the consistency relations are enforced, we can always trade ϵ_k for r_T so that for a typical value $r_T = \mathcal{O}(0.06)$ the value of $\overline{\nu}_{\rm max}$ becomes[29]

$$\overline{\nu}_{\rm max} = 271.88\mathcal{C}(g_s, g_\rho)\left(\frac{\mathcal{A}_\mathcal{R}}{2.41\times 10^{-9}}\right)^{1/4}\left(\frac{r_T}{0.06}\right)^{1/4} \times \left(\frac{h_0^2\Omega_{R0}}{4.15\times 10^{-5}}\right)^{1/4} \text{MHz}. \tag{A14}$$

The frequency $\nu_{\rm max}$ be complemented by the other frequencies of the spectrum and since $\overline{\nu}_{\rm max}$ depends on r_T, also all the other frequencies are sensitive to the specific value of the tensor-to-scalar ratio. Let us then suppose that, before radiation dominance, the postinflationary epoch consists of thee separate phases; this means that the final spectrum is characterized by three typical frequencies: $\nu_1 = \nu_{\rm max}$, ν_2 and $\nu_3 = \nu_r$. The expression of $\nu_{\rm max}$ follows from Eq. (A11) in the case $n = 3$

$$\nu_{\rm max} = \nu_1 = \prod_{i=1}^{2} \xi_i^{\frac{\delta_i - 1}{2(\delta_i+1)}} \overline{\nu}_{\rm max}. \tag{A15}$$

Similarly we can easily compute ν_2 and ν_r:

$$\nu_2 = \sqrt{\xi_1}\xi_2^{(\delta_2-1)/[2(\delta_2+1)]}\overline{\nu}_{\rm max}, \qquad \nu_r = \nu_3 = \sqrt{\xi_1}\sqrt{\xi_2}\overline{\nu}_{\rm max} = \sqrt{\xi}\overline{\nu}_{\rm max}, \tag{A16}$$

where, by definition, $\xi = \xi_1\xi_2$. In the case of n intermediate phases taking place prior to a_r the generic intermediate frequency ν_m can be expressed as

$$\nu_m = \sqrt{\xi_1}\ldots\sqrt{\xi_{m-1}}\prod_{m=1}^{n-1}\xi_i^{\frac{\delta_i-1}{2(\delta_i+1)}}\overline{\nu}_{\rm max}, \tag{A17}$$

$$\nu_r = \nu_n = \sqrt{\xi_1}\sqrt{\xi_2}\ldots\sqrt{\xi_{n-2}}\sqrt{\xi_{n-1}}\overline{\nu}_{\rm max}. \tag{A18}$$

Recalling the remarks presented before Eq. (A5), since the different phases must not last below H_r, the product of all the ξ_i equals H_r/H_1, i.e. by definition $\xi_1\xi_2\ldots\xi_{n-1}\xi_n = \xi = H_r/H_1$. Therefore, in case the consistency relations are enforced, Eqs. (A15)–(A18) show that both the maximal and the intermediate frequencies of the spectrum depend on r_T through ξ.

APPENDIX B: THE EXPANSION RATE AT HORIZON CROSSING

The value of the expansion rate when the wavelengths associated with the pivot wave number k_p cross the comoving Hubble radius determines both the number of e-folds and the typical frequencies of the spectrum. In the present investigation the wavelengths $\mathcal{O}(2\pi/k_p)$ are referred to as the CMB wavelengths. Since at horizon crossing $(H_k/H_1) = \mathcal{O}(1)$ it is natural to set $H_k = \mathcal{O}(H_1)$ in the expressions of N_k and $N_{\rm max}$ [see Eqs. (A8)–(A10) and discussion therein]. If $H_k/H_1 = \mathcal{O}(1)$, then it also follows that $V_1^{1/4}/H_k \gg 1$ where V_1 denotes throughout

[29] As already mentioned in connection with N_k and $N_{\rm max}$, for typical values of the relativistic degrees of freedom, $\mathcal{C}(g_s, g_\rho) = \mathcal{O}(0.75)$. More precisely for $g_{s,eq} = g_{\rho,eq} = 3.94$ and $g_{s,r} = g_{\rho,r} = 106.75$ we have, from Eq. (A13), that $\overline{\nu}_{\rm max} = 148.41$ MHz while $\overline{\nu}_{\rm max} = 206.53$ MHz from Eq. (A14).

this appendix the value of the inflaton potential at H_1. If the estimates are presented in terms of $V_1^{1/4}/H_k$, then the values of N_k and $N_{\rm max}$ are systematically larger than in the case where H_k is measured in units of H_1. In this appendix we also take the opportunity of introducing the relevant notations that are employed throughout the main discussion; in particular, at the end of this appendix the scale dependence of the slow-roll parameters is explicitly analyzed since the related results are relevant for various examples discussed in the text.

1. The role of H_k and H_1

It is well known that the power spectrum of curvature inhomogeneities during inflation can be expressed in two complementary ways:

$$P_{\mathcal{R}}(k,\tau)=\frac{|k\tau|^2}{\pi\epsilon(\tau)}\frac{H^2(\tau)}{M_P^2}\equiv\frac{|k\tau|^2}{\pi\epsilon[\varphi(\tau)]}\frac{H[\varphi(\tau)]}{M_P^2}. \tag{B1}$$

The difference between the first and second equality of Eq. (B1) is that the Hubble rate and the slow-roll parameter ϵ are regarded either as functions of the conformal time coordinate or rather as functionals of the inflaton field φ. When the given wavelength crosses the Hubble radius [i.e. $k\tau=\mathcal{O}(1)$] the previous expression can be written as

$$P_{\mathcal{R}}(k,1/k)=\frac{1}{\pi\epsilon_k}\frac{H_k^2}{M_P^2},\qquad H_k=H(1/k),\qquad \epsilon_k=\epsilon(1/k), \tag{B2}$$

where H_k denotes expansion rate at horizon crossing. We now consider the crossing of the scales relevant for CMB physics and, for these scales, the power spectrum of curvature inhomogeneities is customarily expressed as $P_{\mathcal{R}}(k,1/k)=\mathcal{A}_{\mathcal{R}}(k/k_p)^{n_s-1}$ where k_p is the (conventional) pivot scale while n_s is the (scalar) spectral index. If k is comparable with k_p, then we therefore have that

$$\frac{H_k}{M_P}\simeq\sqrt{\pi\epsilon_k\mathcal{A}_{\mathcal{R}}}=\frac{\sqrt{\pi r_T\mathcal{A}_{\mathcal{R}}}}{4}. \tag{B3}$$

The second expression of Eq. (B3) follows from the consistency relations; we also note that, by definition, in Eq. (B3) $r_T=r_T(k_p)$. If we assume that $r_T\leq 0.03$ and $\mathcal{A}_{\mathcal{R}}=\mathcal{O}(10^{-9})$ it is clear that $H_k/M_P\ll 1$. However it turns out that $H_k=\mathcal{O}(H_1)$ and from the physical viewpoint it is easy to see that $H_k=\mathcal{O}(H_1)$ since the expansion rate decreases very little during inflation. We want however to be more specific and eventually compare H_1/H_k with $V_1^{1/4}/H_k$. From $a_kH_k=k$ we can actually obtain the following chain of equalities:

$$H_k=\frac{H_1}{1-\epsilon_k}\left|\frac{k}{a_1H_1}\right|^{-\frac{\epsilon_k}{1-\epsilon_k}}=H_1\left|\frac{k}{a_1H_1}\right|^{-\epsilon_k}[1+\mathcal{O}(\epsilon_k)]. \tag{B4}$$

But for typical wave numbers $k=\mathcal{O}(k_p)$ it turns out that $k\ll|a_1H_1|$; more specifically we can estimate the value of $k_p/(a_1H_1)$ and obtain

$$\frac{k_p}{a_1H_1}=\frac{10^{-25.85}}{\mathcal{D}(\delta_i,\xi_i)}\left(\frac{k_p}{0.002\ \mathrm{Mpc}^{-1}}\right)\left(\frac{r_T}{0.03}\right)^{-1/4}\times\left(\frac{\mathcal{A}_{\mathcal{R}}}{2.41\times10^{-9}}\right)^{-1/4}\left(\frac{h_0^2\Omega_{R0}}{4.15\times10^{-5}}\right)^{-1/4}. \tag{B5}$$

For a postinflationary history dominated by radiation all the δ_i go to 1 and $k_p=\mathcal{O}(10^{-26})a_1H_1$ and when the expansion rate is slower than radiation the ratio $k_p/(a_1H_1)$ is even smaller. Therefore, if we insert Eq. (B5) into Eq. (B4), we can conclude, as previously anticipated in Eq. (A5), that

$$\frac{H_k}{M_P}\simeq\sqrt{\pi\epsilon_k\mathcal{A}_{\mathcal{R}}},\qquad H_k\simeq H_1. \tag{B6}$$

Even if, according to Eq. (B6), H_k and H_1 are of the same order, V_1^1 and H_k are rather different. To appreciate this statement we recall that, at the end of inflation, $\epsilon\to1$ which means $H^2=-\dot{H}$; but this condition can also be translated as $V=\dot{\varphi}^2$ and this implies that $H_1^2M_P^2=4\pi V_1$. We can therefore obtain an estimate of $V_1^{1/4}$ and the result is

$$\frac{V_1^{1/4}}{H_k}=\frac{\sqrt{H_1/H_k}}{\sqrt{2\pi}(\epsilon_k\mathcal{A}_{\mathcal{R}})^{1/4}}\gg1. \tag{B7}$$

If we use Eq. (B7) and express N_k in terms of $V_1^{1/4}/H_k$ we get

$$N_k=64.902+\ln\left[\frac{\mathcal{C}(g_s,g_\rho)}{0.7596}\right]-\ln\left(\frac{k}{0.002\ \mathrm{Mpc}^{-1}}\right)+\frac{1}{4}\ln\left(\frac{h_0^2\Omega_{R0}}{4.15\times10^{-5}}\right)+\frac{1}{2}\sum_i^{n-1}\left(\frac{\delta_i-1}{\delta_i+1}\right)\times\ln\xi_i-\ln\left(\frac{V_1^{1/4}}{H_k}\right). \tag{B8}$$

If we compare Eqs. (A10) and (B8) we see that, because of Eq. (B7), the value of N_k gets larger than in the case where the number of e-folds is expressed as a function of H_k/H_1; since $H_k/H_1=\mathcal{O}(1)$, Eq. (A10) is more suitable for an explicit estimate of N_k.

2. Specific potentials and slow-roll algebra

When the consistency relations are enforced the tensor to scalar ratio cannot be equally small for all the classes of inflationary potentials and while the monomials are clearly

excluded, the plateaulike and the hilltop potentials may lead to r_T that are comparatively smaller. Since different classes of potentials have been mentioned in the main discussion, their associated properties will now be swiftly recalled. In the case of Eq. (2.37) the explicit expressions of the slow-roll parameters follow from Eq. (2.34) so $\epsilon(\Phi)$ and $\overline{\eta}(\Phi)$ are given by

$$\epsilon(\Phi) = \frac{2q^2}{\Phi^2(1+\beta^2\Phi^{\frac{4q}{p}})^2},$$
$$\overline{\eta}(\Phi) = \frac{2q[2pq - p - \beta^2(p+4q)\Phi^{\frac{4q}{p}}]}{p\Phi^2(1+\beta^2\Phi^{\frac{4q}{p}})^2}. \tag{B9}$$

In this case, according to Eq. (B9), the tensor-to-scalar ratio and the scalar spectral index are given by

$$r_T(\Phi) = \frac{32q^2}{\Phi^2(1+\beta^2\Phi^{\frac{4q}{p}})^2},$$
$$n_s(\Phi) = 1 - \frac{4pq(1+q) + 4q(q+4p)\beta^2\Phi^{\frac{4q}{p}}}{p\Phi^2(1+\beta^2\Phi^{\frac{4q}{p}})^2}. \tag{B10}$$

To compare the physical features of the various potentials when the pivot scales cross the comoving Hubble radius it is practical to estimate directly ϵ_k and $\overline{\eta}_k$ as a function of the number of e-folds N_k for $k = \mathcal{O}(k_p)$. For this purpose, as a a general observation, we should compute the total number of e-folds elapsed since the crossing of the bunch of the CMB wavelengths; since this procedure is consistently followed for all the explicit potentials discussed here, it is useful to discuss it more explicitly in the concrete case of Eq. (2.37). The number of e-folds N_k is then given by

$$N_k = \int_{\Phi_f}^{\Phi_k}\left(\frac{v}{\partial_\Phi v}\right)d\Phi = \int_{\Phi_f}^{\Phi_k}\frac{\Phi}{2q}(1+\beta^2\Phi^{\frac{4q}{p}})d\Phi, \tag{B11}$$

where Φ_k denotes the value of the field when the scale k crosses the comoving Hubble radius while $\Phi_f \to 1$ coincides with the end of inflation. Even if, as we saw, different approaches can be envisaged we are here taking the standard practice and require that

$$\epsilon(\Phi_f) \to 1 \Rightarrow H^2 = -\dot{H} \Rightarrow V = \dot{\varphi}^2. \tag{B12}$$

For instance if we evaluate $\epsilon(\Phi_f)$ from Eq. (B9) and require $\epsilon(\Phi_f) \to 1$ we obtain the condition

$$\Phi_f^2(1+\beta^2\Phi_f^{4q/p})^2 = 2q^2. \tag{B13}$$

We now have two complementary possibilities. If $\beta^2 < 1$ (as we always assumed in the explicit evaluations) then $\Phi_f \simeq 1/(\sqrt{2}q) = \mathcal{O}(1)$. In the opposite case (i.e. $\beta > 1$) we get $\Phi_f \simeq (\sqrt{2}q\beta^2)^{q/(4p+q)}$ which is again of order 1. All in all from Eq. (B11) the number of e-folds is ultimately given by

$$N_k = \frac{\Phi_k^2 - 1}{4q} + \frac{p\beta^2(\Phi_k^{2+\frac{4q}{p}} - 1)}{4q(p+2q)}, \tag{B14}$$

where we simply assumed $\Phi_f \to 1$. Since the field value at Φ_k is defined at the time of the crossing during inflation we can take the limit $\Phi_k \gg 1$ in Eq. (B14) and eventually determine the connection between Φ_k and N_k:

$$N_k = \frac{p\beta^2}{4q(p+2q)}\Phi_k^{2+\frac{4q}{p}} \Rightarrow \Phi_k = \left[\frac{4q(p+2q)N_k}{p\beta^2}\right]^{\frac{p}{2(p+2q)}}. \tag{B15}$$

Thanks to Eqs. (B15), (B9) and (B10) can be directly expressed in terms of $\Phi_k > 1$

$$\epsilon_k = \frac{2q^2}{\beta^4\Phi_k^{8q/p+2}}, \qquad \overline{\eta}_k = -\frac{2q(p+4q)}{p\beta^2\Phi_k^{8q/p+2}}. \tag{B16}$$

Finally using Eq. (B15) into Eq. (B16) we have

$$\epsilon_k = \frac{2q^2\beta^{-\frac{2p}{p+2q}}}{[4q(p+2q)N_k/p]^{\frac{p+4q}{p+2q}}}, \quad \overline{\eta}_k = -\frac{p+4q}{2(p+2q)N_k}. \tag{B17}$$

The same strategy is used for the other potentials discussed in Secs. II and IV.

[1] D. N. Spergel *et al.* (WMAP Collaboration), Astrophys. J. Suppl. Ser. **148**, 175 (2003).
[2] D. N. Spergel *et al.* (WMAP Collaboration), Astrophys. J. Suppl. Ser. **170**, 377 (2007).
[3] L. Page *et al.* (WMAP Collaboration), Astrophys. J. Suppl. Ser. **170**, 335 (2007).
[4] P. A. R. Ade *et al.* (Planck Collaboration), Astron. Astrophys. **571**, A16 (2014).
[5] P. A. R. Ade *et al.* (BICEP2 Collaboration), Phys. Rev. Lett. **112**, 241101 (2014).
[6] D. Hanson *et al.* (South Pole Telescope Collaboration), Phys. Rev. Lett. **111**, 141301 (2013).

[7] P. J. E. Peebles and J. T. Yu, Astrophys. J. **162**, 815 (1970).
[8] Y. Akrami *et al.* (Planck Collaboration), Astron. Astrophys. **641**, A10 (2020).
[9] N. Aghanim *et al.* (Planck Collaboration), Astron. Astrophys. **641**, A6 (2020).
[10] P. Ade *et al.* (BICEP and Keck Collaborations), Phys. Rev. Lett. **127**, 151301 (2021).
[11] K. Enqvist, H. Kurki-Suonio, and J. Valiviita, Phys. Rev. D **62**, 103003 (2000).
[12] S. Weinberg, Phys. Rev. D **67**, 123504 (2003).
[13] H. Kurki-Suonio, V. Muhonen, and J. Valiviita, Phys. Rev. D **71**, 063005 (2005).
[14] M. Giovannini, Classical Quantum Gravity **23**, 4991 (2006).
[15] L. P. Grishchuk, Zh. Eksp. Teor. Fiz. **67**, 825 (1974) [Sov. Phys. JETP **40**, 409 (1975)].
[16] L. P. Grishchuk, Ann. N.Y. Acad. Sci. **302**, 439 (1977).
[17] A. A. Starobinsky, JETP Lett. **30**, 682 (1979).
[18] V. A. Rubakov, M. V. Sazhin, and A. V. Veryaskin, Phys. Lett. **115B**, 189 (1982).
[19] L. P. Grishchuk and M. Solokhin, Phys. Rev. D **43**, 2566 (1991).
[20] M. Giovannini, Phys. Rev. D **58**, 083504 (1998).
[21] M. Giovannini, Phys. Rev. D **60**, 123511 (1999).
[22] M. Giovannini, Classical Quantum Gravity **16**, 2905 (1999).
[23] B. Abbott *et al.* (LIGO Collaboration), Phys. Rev. D **69**, 122004 (2004); Phys. Rev. Lett. **95**, 221101 (2005).
[24] J. Aasi *et al.* (LIGO/Virgo Collaborations), Phys. Rev. Lett. **113**, 231101 (2014); Phys. Rev. D **91**, 022003 (2015).
[25] B. P. Abbott *et al.* (LIGO/Virgo Collaborations), Phys. Rev. Lett. **118**, 121101 (2017); **119**, 029901(E) (2017)]; Phys Rev. D **100**, 061101(R) (2019).
[26] R. Abbott *et al.* (KAGRA, Virgo, and LIGO Scientific Collaborations), Phys. Rev. D **104**, 022004 (2021).
[27] Z. Arzoumanian *et al.* (NANOGrav Collaboration), Astrophys. J. Lett. **905**, L34 (2020); N. S. Pol *et al.* (NANOGrav Collaboration), Astrophys. J. Lett. **911**, L34 (2021).
[28] B. Goncharov *et al.*, Astrophys. J. Lett. **917**, L19 (2021).
[29] S. Chen *et al.*, Mon. Not. R. Astron. Soc. **508**, 4970 (2021).
[30] J. Antoniadis *et al.*, Mon. Not. R. Astron. Soc. **510**, 4873 (2022).
[31] V. F. Schwartzman, Pis'ma Zh. Eksp. Teor. Fiz. **9**, 315 (1969) [JETP Lett. **9**, 184 (1969)].
[32] M. Giovannini, H. Kurki-Suonio, and E. Sihvola, Phys. Rev. D **66**, 043504 (2002).
[33] R. Cyburt, B. D. Fields, K. A. Olive, and E. Skillman, Astropart. Phys. **23**, 313 (2005).
[34] M. Giovannini, Phys. Lett. B **668**, 44 (2008).
[35] M. Giovannini, Phys. Rev. D **100**, 083531 (2019).
[36] L. H. Ford and L. Parker, Phys. Rev. D **16**, 1601 (1977).
[37] D. R. Brill and J. B. Hartle, Phys. Rev. **135**, B271 (1964).
[38] R. A. Isaacson, Phys. Rev. **166**, 1263 (1968); **166**, 1272 (1968).
[39] M. Giovannini, Prog. Part. Nucl. Phys. **112**, 103774 (2020).
[40] V. N. Lukash, Zh. Eksp. Teor. Fiz. **79**, 1601 (1980) [Sov. Phys. JETP **52**, 807 (1980)].
[41] M. Giovannini, Phys. Rev. D **88**, 021301 (2013).
[42] M. Giovannini, Phys. Rev. D **89**, 123517 (2014).
[43] M. S. Turner, Phys. Rev. D **28**, 1243 (1983).
[44] S. S. Mishra, V. Sahni, and A. A. Starobinsky, J. Cosmol. Astropart. Phys. 05 (2021) 075.
[45] A. Ijjas, P. J. Steinhardt, and A. Loeb, Phys. Lett. B **723**, 261 (2013).
[46] A. Ijjas, P. J. Steinhardt, and A. Loeb, Phys. Lett. B **736**, 142 (2014).
[47] R. Easther, B. Bahr-Kalus, and D. Parkinson, Phys. Rev. D **106**, L061301 (2022).
[48] L. Boubekeur and D. H. Lyth, J. Cosmol. Astropart. Phys. 07 (2005) 010.
[49] N. K. Stein and W. H. Kinney, J. Cosmol. Astropart. Phys. 03 (2023) 027.
[50] H. Motohashi and A. A. Starobinsky, J. Cosmol. Astropart. Phys. 11 (2019) 025.
[51] M. Guerrero, D. Rubiera-Garcia, and D. Saez-Chillon Gomez, Phys. Rev. D **102**, 123528 (2020).
[52] A. Mohammadi, T. Golanbari, S. Nasri, and K. Saaidi, Phys. Rev. D **101**, 123537 (2020).
[53] L. Dai, M. Kamionkowski, and J. Wang, Phys. Rev. Lett. **113**, 041302 (2014).
[54] J. B. Munoz and M. Kamionkowski, Phys. Rev. D **91**, 043521 (2015).
[55] J. L. Cook, E. Dimastrogiovanni, D. A. Easson, and L. M. Krauss, J. Cosmol. Astropart. Phys. 04 (2015) 047.
[56] M. Giovannini, Phys. Rev. D **89**, 123517 (2014).
[57] S. Mishra, V. Sahni, and A. Starobinsky, J. Cosmol. Astropart. Phys. 05 (2021) 075.
[58] A. Chakraborty, M. R. Haque, D. Maity, and R. Mondal, Phys. Rev. D **108**, 023515 (2023).
[59] M. Giovannini, Classical Quantum Gravity **26**, 045004 (2009).
[60] W. H. Kinney, arXiv:2103.00281.
[61] M. Giovannini, Phys. Rev. D **105**, 103524 (2022).
[62] P. J. E. Peebles and A. Vilenkin, Phys. Rev. D **59**, 063505 (1999).
[63] L. H. Ford, Phys. Rev. D **35**, 2955 (1987).
[64] B. Spokoiny, Phys. Lett. B **315**, 40 (1993).
[65] J. Haro, W. Yang, and S. Pan, J. Cosmol. Astropart. Phys. 01 (2019) 023.
[66] M. Gorghetto, E. Hardy, and H. Nicolaescu, J. Cosmol. Astropart. Phys. 06 (2021) 034.
[67] B. Li and P. R. Shapiro, J. Cosmol. Astropart. Phys. 10 (2021) 024.
[68] S. Weinberg, Phys. Rev. D **69**, 023503 (2004).
[69] D. A. Dicus and W. W. Repko, Phys. Rev. D **72**, 088302 (2005).
[70] H. X. Miao and Y. Zhang, Phys. Rev. D **75**, 104009 (2007).
[71] B. A. Stefanek and W. W. Repko, Phys. Rev. D **88**, 083536 (2013).
[72] K. W. Ng, Phys. Rev. D **86**, 103510 (2012).
[73] M. S. Turner, M. J. White, and J. E. Lidsey, Phys. Rev. D **48**, 4613 (1993).
[74] L. M. Krauss and M. J. White, Phys. Rev. Lett. **69**, 869 (1992).
[75] M. Giovannini, J. Cosmol. Astropart. Phys. 05 (2023) 056.
[76] F. Pegoraro, L. Radicati, Ph. Bernard, and E. Picasso, Phys. Lett. **68A**, 165 (1978).
[77] F. Pegoraro, E. Picasso, and L. Radicati, J. Phys. A **11**, 1949 (1978).
[78] C. M. Caves, Phys. Lett. **80B**, 323 (1979).

[79] C. Reece, P. Reiner, and A. Melissinos, Nucl. Instrum. Methods Phys. Res., Sect. A **245**, 299 (1986).
[80] Ph. Bernard, G. Gemme, R. Parodi, and E. Picasso, Rev. Sci. Instrum. **72**, 2428 (2001).
[81] R. Ballantini, P. Bernard, A. Chincarini, G. Gemme, R. Parodi, and E. Picasso, Classical Quantum Gravity **21**, S1241 (2004).
[82] V. B. Braginsky and M. B. Menskii, Pis'ma Zh. Eksp. Teor. Fiz. **13**, 585 (1971) [JETP Lett. **13**, 417 (1971)].
[83] V. B. Braginsky, L. P. Grishchuk, A. G. Doroshkevich, Ya. B. Zeldovich, I. D. Novikov, and M. Sazhin, Zh. Eksp. Teor. Fiz. **65**, 1729 (1973) [Sov. Phys. JETP **38**, 865 (1974)].
[84] A. M. Cruise, Classical Quantum Gravity **17**, 2525 (2000).
[85] A. M. Cruise and R. M. Ingley, Classical Quantum Gravity **23**, 6185 (2006).
[86] F. Y. Li, M. X. Tang, and D. P. Shi, Phys. Rev. D **67**, 104008 (2003).
[87] A. Nishizawa *et al.*, Phys. Rev. D **77**, 022002 (2008).
[88] S. Dimopoulos, P. Graham, J. Hogan, M. Kasevich, and S. Rajendran, Phys. Rev. D **78**, 122002 (2008).
[89] S. Dimopoulos, P. W. Graham, J. M. Hogan, M. A. Kasevich, and S. Rajendran, Phys. Lett. B **678**, 37 (2009).
[90] A. R. Liddle and S. M. Leach, Phys. Rev. D **68**, 103503 (2003).